J. Fluid Mech. (1991), *vol.* 228, *pp.* 207–241
Printed in Great Britain

On the dynamics of suspended microstructure in unsteady, spatially inhomogeneous, two-dimensional fluid flows

By ANDREW J. SZERI[1], STEPHEN WIGGINS[2] AND L. GARY LEAL[1]

[1] Department of Chemical and Nuclear Engineering, University of California, Santa Barbara, CA 93106, USA

[2] Applied Mechanics, California Institute of Technology, Pasadena, CA 91125, USA

(Received 17 April 1990 and in revised form 6 December 1990)

The dynamical behaviour of stretchable, orientable microstructure suspended in a general two-dimensional fluid flow is investigated. The state of the microstructure in question is described by an axial vector; thus the microstructure may consist of axisymmetric particles, droplets of fluid, models of polymer molecules or simply a line element of the fluid itself. A quantitative measure is developed to distinguish conformation(s) (orientations and stretched lengths) of the microstructure that are robust and attractive. This leads to a strong flow criterion for microstructure suspended in unsteady, spatially inhomogeneous flows in which the effects of history-dependence are apparent. The important special case where the influence of the flow on the microstructure is time periodic is considered in some detail, owing to the fact that one can obtain additional results that concern orientation dynamics. Finally, several examples are given which illustrate the application of the present methods and the relevant innovations of the approach. Throughout the analysis, special attention is given to the robustness of the dynamics to changes in the modelling assumptions such as slight three-dimensionality or Brownian diffusion, etc. The results of the study demonstrate that using microdynamical behaviour in steady, homogeneous flows to derive macroscopic properties (such as strong flow criteria) which are then applied to problems in unsteady, spatially inhomogeneous flows can lead to incorrect results. Instead, one must account properly for effects due to the history of the flow.

1. Introduction

The macroscopic properties of heterogeneous fluids that contain particles, drops, or molecules depend on the state of the conformation, by which we generally mean the concentration distribution and the degree of orientation, stretch or other measures of departure from the equilibrium state. In this paper, we assume that the heterogeneous phase is uniformly distributed, and that its conformation can be described by a single vector. Strictly speaking, a vector description is possible only if the microstructure is axisymmetric, but we may hope that the theory can also be applied to systems that adopt an elongated but non-axisymmetric shape. The time-dependent behaviour of this class of microstructural fluids thus includes a number of important problems. For example, the stretching of droplets is related to the break-up or emulsification problem. Macromolecular stretching and orientation is thought

to be a contributory factor in drag reduction in extremely dilute solutions of polymer molecules. Finally, the dynamical behaviour of orientable filler particles in polymer liquids is important in the plastics manufacturing industry.

Past studies of the dynamics of such systems have focused on the behaviour of microstructure in steady, homogeneous flows, which we refer to hereinafter as *simple flows*. By definition, simple flows have a velocity gradient tensor field which is constant in both time and space. The time evolution of stretch and orientation of the microstructure in simple flows is governed by a system of autonomous differential equations. These equations can be solved analytically as shown by previous investigators (and reviewed in §2).

In spite of the fact that an analytical solution is available, however, most researchers have not concentrated on the dynamics of stretch and orientation, but rather on the initiation of stretching of the microstructure. Such an investigation leads to flow classification schemes on the basis of whether or not a flow is capable of initiating stretch (cf. Tanner & Huilgol 1975; Tanner 1976; Astarita 1979; Olbricht, Rallison & Leal 1982; Nollert & Olbricht 1985). Primarily these efforts are aimed at developing a 'strong flow criterion', by which is meant a sufficient condition for the onset of stretching of the microstructure. The methods employed are those of linear stability analysis.

The dynamical behaviour of microstructure in spatially inhomogeneous or time-dependent flows, hereinafter termed *complex*, is much richer. Whereas simple flows lead to autonomous dynamical equations, complex flows lead to non-autonomous dynamical equations, i.e. systems with time-dependent forcing. Recall that in autonomous differential equations, the independent variable does not enter into the equation explicitly; it enters only implicitly through derivatives. Non-autonomous equations contain explicit dependence on the independent variable.

Clues about the richness of the dynamics of microstructural fluids in complex flows can be found in James & Saringer (1982), who examined the flow of a solution of macromolecules through small orifices. They found that the strain rate for onset of stretching of the macromolecules depended strongly on the shape of the orifice, thus implicitly on the history of the flow field experienced by the macromolecule. One might argue that this phenomenon can be explained by 'intelligent' application of the strong-flow criterion for simple flows, which would respect the time intervals over which the microstructure experiences the pre-shearing and extensional flows. However, no systematic way of accomplishing this has yet emerged. In the present analysis, we demonstrate that the fault lies not in the application of the strong-flow criterion, but in the strong-flow criterion itself. The problem is that the spatially inhomogeneous nature of the velocity field (in this instance) is ignored in the development of conventional strong-flow criteria.

Such manifestations of history-dependent behaviour were also discussed by Nollert & Olbricht (1985), who analysed a dumb-bell model for macromolecules in periodic extensional flows suggestive of flows in porous media. They found that when the velocity gradient (following the particle) is unsteady, the kinematic history of the microstructure can strongly affect the conditions required for stretching of the particles at any instant. However, in their analysis, Nollert & Olbricht approximate smoothly (spatially) varying velocity fields of the surrounding flow by sequences of steady flow fields with step changes between consecutive members of the sequence. This is equivalent to approximating a non-autonomous differential equation by a sequence of autonomous equations. We give several graphic demonstrations of the fact that this approach can lead to qualitatively incorrect results. In fact, Nollert &

Olbricht themselves give an example (their figure 8) in which they compare the end-to-end length of the dumb-bell model in flows that change continuously and in 'equivalent' flows where the time-dependence is modelled as a sequence of steady flows. The latter approximation yields errors of 30% for the particular case they consider. Thus the details of the history are important to the response of microstructural elements.

In this paper, we examine the dynamics of microstructure, as described by a model dynamical equation, in complex, two-dimensional flows that are time-dependent in a frame of reference that moves with the microstructure. We are careful to treat the resultant non-autonomous system of equations in a mathematically correct fashion, although we find it necessary to develop some new tools as we go along. The model system that we treat corresponds to an exact microdynamical equation for some types of microstructure and to an approximate model for other types of microstructure. In the model system, it is assumed that the microstructure is small compared to the lengthscale over which the surrounding fluid flow changes. Moreover, we restrict the analysis to the case of two-dimensional flow. Through careful analysis of the structure of the evolution equations, we show that it is possible to indicate whether or not a slight relaxation of the basic model assumptions will change the dynamics in a qualitative way. We emphasize that flow-microstructure systems described by different microdynamical equations will show the same qualitative differences in behaviour between simple and complex flows as are shown here for our particular model system.

The main thesis of the present paper is that the non-autonomous nature of the conformation evolution equations in complex flows leads to history-dependent behaviour that cannot be approximated by the autonomous behaviour in simple flows, or in a sequence of simple flows, as some have suggested. The primary results of our analysis are: (i) a necessary and sufficient condition for stretching of microstructure (i.e. a 'strong flow criterion') in complex flows that takes history properly into account; and (ii) conditions for the existence of *time-dependent attractors* for the orientation dynamics of microstructure in complex flows, that are analogous to steady, equilibrium orientations for microstructure in simple flows.

In order to understand the differences between microdynamics in simple and complex flow, we begin in §2 with a careful analysis of the dynamics of microstructure in simple flows. In §3 we give the analysis that leads to our history-dependent strong-flow criterion, which may be applied to microstructure in any two-dimensional flow. In §4 we demonstrate that history-dependence in time-periodic flows can lead to attractors in the orientation dynamics. Finally, we give examples of these history-dependent flow phenomena in §5 and our conclusions in §6. In an Appendix, we discuss the relation of our methods to those of conventional dynamical stability analysis.

2. Equations of motion

Exact microdynamical equations for different types of axisymmetric particles have been derived by many researchers. Rigid particles were examined by Bretherton (1962), elastic ellipsoidal particles by Hinch (1977), linear elastic dumb-bell models for the dynamics of dilute polymer solutions by Kuhn & Kuhn (1945), and linear elastic dumb-bells with internal viscosity by Bird *et al.* (1987). As demonstrated by Olbricht *et al.* (1982), all of these dynamical equations may be collapsed into a single

equation for the state vector, with the various specific physical systems corresponding to particular values of the model parameters:

$$\dot{\boldsymbol{R}} = \boldsymbol{\Omega}\cdot\boldsymbol{R} + G\left[\boldsymbol{E}\cdot\boldsymbol{R} - \frac{F}{F+1}\frac{\boldsymbol{R}\cdot\boldsymbol{E}\cdot\boldsymbol{R}}{\|\boldsymbol{R}\|^2}\boldsymbol{R}\right] - \frac{\alpha}{F+1}\boldsymbol{R}. \tag{2.1}$$

We discuss the relevant lengthscales of the microstructure and flow, below. The orientation and length of the microstructure are given by the state vector $\boldsymbol{R}$. $\boldsymbol{\Omega}$ and $\boldsymbol{E}$ are the vorticity and rate-of-strain tensors, respectively, and the parameters G, α and F correspond to the shape factor, the elastic modulus of the internal spring and the internal viscosity of the microstructure, respectively. Parameter values that yield the microdynamical equations for each particular physical system referred to above can be found in Olbricht *et al.* (1982). For our purposes, it is sufficient to note that $\alpha \geqslant 0$, $F \geqslant 0$ and G is generally between 0 and 1, although it may exceed 1 for certain particles, as shown by Bretherton (1962). It is also worth noting that $G = 1$, $\alpha = F = 0$ yields an equation for microstructure that rotates and stretches as an infinitesimal line element of the fluid. For this latter reason, the present analysis has application in the study of mixing where the microstructure may be taken to be an infinitesimal line element of an interface between two fluids, for example.

Equation (2.1) describes the time evolution of the orientation and stretching of the microstructure, under the assumption that the lengthscale of the microstructural elements is large compared to the continuum limit of the suspending fluid but small compared to some suitably defined lengthscale of the flow. Thus its evolving orientation and length change in response to the local vorticity and rate-of-strain of the surrounding fluid flow. Indeed, because the microstructure is smaller than the lengthscale over which $\boldsymbol{\Omega}$ and $\boldsymbol{E}$ change, one might be tempted to approximate $\boldsymbol{\Omega}$ and $\boldsymbol{E}$ as constant, or at least as piecewise-constant along the particle path. However, this practice is inconsistent with the dynamics of microstructure even in slowly varying flow fields, as we show by example in §§3.1 and 5.2.

In practical problems one must be concerned with interactions of the elements of the microstructure with solid boundaries and with other elements of the microstructure. This introduces other lengthscales that we do not consider here. In practice, the useful range of microstructure lengthscale normally extends over several orders of magnitude. We remark that (2.1) permits evolution of the state vector to a state of zero or infinite length. At these extremes, however, the modelling assumptions implicit in (2.1) break down. One may rectify one problem by including Brownian motion, which prevents $|\boldsymbol{R}| \to 0$, and the other by replacing the linear spring by a nonlinear spring, which prevents $|\boldsymbol{R}| \to \infty$. However, for the purposes of this study, the simple model system (2.1) will suffice.

If the microstructure should be placed in a flow in which $\boldsymbol{\Omega}$ and $\boldsymbol{E}$ do not change along the particle path, i.e. when $\boldsymbol{\Omega}$ and $\boldsymbol{E}$ are constant tensors (simple flow), then (2.1) is an autonomous ordinary differential equation with an easily obtained solution that we review below. When $\boldsymbol{\Omega}$ and $\boldsymbol{E}$ change along the particle path, i.e. when $\boldsymbol{\Omega}$ and $\boldsymbol{E}$ evaluated along the particle path are time dependent (complex flow), then (2.1) is non-autonomous and therefore much more difficult to analyse.

2.1. *Coordinate form of the evolution equation*

The model system, equation (2.1), describes the time evolution of the state of microstructure in unsteady, spatially inhomogeneous, three-dimensional fluid flow. For simplicity, we shall confine our analysis to the special case of incompressible, two-dimensional fluid flows. The principal simplifications that result from this

restriction are (i) that the vorticity tensor is described by a single scalar quantity (rather than three), and (ii) that the rate-of-strain tensor is described by two scalar quantities (rather than five). This is a strong restriction of the flow. However, as we show below, one can determine when the results we obtain for purely two-dimensional flows will apply to almost two-dimensional flows. In fact, the same analysis tests the dynamics obtained from the model system for sensitivity to other changes in the model equation, which might be due to Brownian diffusion, nonlinear effects, etc.

We consider two-dimensional fluid flows; thus it is convenient to work in a rectangular coordinate system (x, y, z) in which the flow takes place in the (x, y)-plane. Normally, one would treat this problem in a coordinate system chosen to coincide with the principal axes of the rate-of-strain tensor. However, this proves to be a cumbersome approach in the complex flow problems we treat below because the orientations of these principal axes change from point to point in space and possibly also in time. For unity of presentation, therefore, we shall use general rectangular coordinates for both the simple and complex flows.

The instantaneous orientation of the state vector $\boldsymbol{R}$ is therefore described with respect to the coordinate system (x, y, z). Because this coordinate system is not rotating, there is no danger of introducing non-physical effects.

Let the orientation of the microstructure be given by its angle σ with the x-axis and by the angle θ measured from the (x, y)-plane. If the length of the particle is ρ, then in the rectangular coordinates (x, y, z), the state vector of the microstructure is

$$\boldsymbol{R} = \begin{pmatrix} \rho\cos\theta\cos\sigma \\ \rho\cos\theta\sin\sigma \\ \rho\sin\theta \end{pmatrix}. \tag{2.2}$$

These variables are shown in the definition sketch of figure 1. Note that we are not using standard spherical polar coordinates to describe the orientation of the microstructure because it is convenient to have $\theta = 0$ correspond to the alignment of the state vector of the microstructure in the plane of the (two-dimensional) flow.

The vorticity and rate-of-strain tensors in the rectangular coordinate system can be written in the form:

$$\boldsymbol{\Omega} = \begin{bmatrix} 0 & -\frac{1}{2}\omega & 0 \\ \frac{1}{2}\omega & 0 & 0 \\ 0 & 0 & 0 \end{bmatrix}, \quad \boldsymbol{E} = \begin{bmatrix} e & \frac{1}{2}\gamma & 0 \\ \frac{1}{2}\gamma & -e & 0 \\ 0 & 0 & 0 \end{bmatrix}. \tag{2.3), (2.4}$$

Because the forms (2.3), (2.4) are valid whether the tensors are time dependent or not, the evolution equations we derive in this section can be applied to both simple and complex flows. As the fluid flows we consider are planar, we can make use of the stream function $\psi = \psi(x, y, t)$. The flow parameters appearing in (2.3), (2.4) are the vorticity

$$\omega = -\frac{\partial^2\psi}{\partial x^2} - \frac{\partial^2\psi}{\partial y^2}, \tag{2.5}$$

the elongation e and the shear γ.

$$e = \frac{\partial^2\psi}{\partial x\,\partial y}, \quad \gamma = \frac{\partial^2\psi}{\partial y^2} - \frac{\partial^2\psi}{\partial x^2}. \tag{2.6a, b}$$

Note that if we were working in the principal axes of the rate-of-strain tensor, the quantity γ would be zero, and the parameters e and ω take different values. Also we

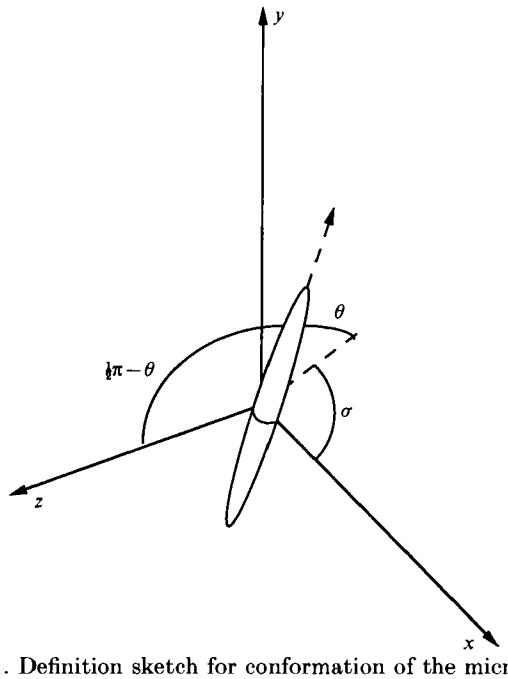

FIGURE 1. Definition sketch for conformation of the microstructure.

would have an additional flow parameter which indicated the inclination of the principal strain axes with respect to some external reference frame. However, we do not choose to work in such coordinates for the reasons we have outlined above.

Physically, the flow parameters may be interpreted as follows. The local rigid rotation rate of the flow is given by half the vorticity ω. Locally, the flow also consists of a pure straining motion described by the pair of flow parameters e and γ. The principal axes of the straining motion are in the directions

$$\boldsymbol{s}_1 = \frac{-\gamma}{2e-(4e^2+\gamma^2)^{\frac{1}{2}}}\boldsymbol{e}_x+\boldsymbol{e}_y, \quad \boldsymbol{s}_2 = \frac{-\gamma}{2e+(4e^2+\gamma^2)^{\frac{1}{2}}}\boldsymbol{e}_x+\boldsymbol{e}_y.$$

The rate-of-strain in each direction is $s_{\max} = (e^2+\frac{1}{4}\gamma^2)^{\frac{1}{2}}$ and $s_{\min} = -(e^2+\frac{1}{4}\gamma^2)^{\frac{1}{2}}$, respectively.

Now we substitute (2.2)–(2.4) into the evolution equation (2.1). To separate the different components of the result, we take the inner product with the vectors

$$\frac{1}{\rho\cos\theta}\begin{pmatrix}-\sin\sigma\\ \cos\sigma\\ 0\end{pmatrix}, \quad \frac{1}{\rho}\begin{pmatrix}\sin\theta\cos\sigma\\ \sin\theta\sin\sigma\\ -\cos\theta\end{pmatrix}, \quad \begin{pmatrix}\cos\theta\cos\sigma\\ \cos\theta\sin\sigma\\ \sin\theta\end{pmatrix}.$$

Mathematically, this is equivalent to taking the projection of $\mathrm{d}\boldsymbol{R}/\mathrm{d}t$ along the directions in which the coordinates σ, θ and ρ are increasing. This yields separate evolution equations for σ, θ and ρ, respectively:

$$\dot{\sigma} = \tfrac{1}{2}\omega - Ge\sin 2\sigma + \tfrac{1}{2}G\gamma\cos 2\sigma, \tag{2.7a}$$

$$\dot{\theta} = -\tfrac{1}{2}G(e\cos 2\sigma + \tfrac{1}{2}\gamma\sin 2\sigma)\sin 2\theta, \tag{2.7b}$$

$$\dot{\rho} = \left[\frac{G}{F+1}(e\cos 2\sigma + \tfrac{1}{2}\gamma\sin 2\sigma)\cos^2\theta - \frac{\alpha}{F+1}\right]\rho. \tag{2.7c}$$

We remark that in the limit of large F (rigid particle) and for the flow parameters

$e = 0$, $\gamma = -\omega = \lambda$, we recover Jeffrey's (1922) classical equations for the rotation of a rigid spheroid in uniform shear flow, $\psi = \frac{1}{2}\lambda y^2$. Note that the fluid flow exerts an influence on the orientation and stretching through the flow parameters e, γ and ω. In a simple flow, these parameters are constant in time. In this case, (2.7) comprises an autonomous system with a solution that may be obtained by simple integration, as we review below.

Almost all flows, however, are complex. In this case, the flow parameters depend on time through (i) the motion of the microstructure through different physical regions of the flow, and (ii) the changes with time of the flow field as a whole. Thus the system (2.7) is non-autonomous for complex flow fields, and the time dependent flow parameters e, γ and ω may properly be thought of as time-dependent forcing.

2.2. *The dynamics of microstructure in simple flows*

Before we consider the general case of complex flow fields, we review the known results for simple flows. As we have explained, the system of (2.7) is autonomous in this case, with the parameters e, γ and ω constant in time.

The analysis of this section is of importance to the general arguments of the paper. In particular, we demonstrate that the orientation dynamics and strong-flow criteria one derives for microstructure in simple flows are based strongly on the assumption that the microdynamical equations are autonomous. This assumption is buried rather deeply, especially in the strong-flow criteria for microstructure in simple flows that have been derived by many researchers. Our aim in this section is to review the analysis for simple flows in order that it may be clear, later, why microdynamics and strong-flow criteria must be different in complex flows. Along the way, we give analytic solutions of the three equations of motion (2.7) so that understanding a specific example is as simple as fixing the flow parameters e, γ and ω and the microstructure constants G, α and F and plotting the results. In §2.3 we analyse the sensitivity of the solutions to changes in the model system.

We begin by considering the orientation problem (σ, θ), leaving the stretching degree of freedom (ρ) for later. Rather than working with $\sigma(t)$ and $\theta(t)$ as dependent variables with t as the independent variable, it is more convenient to treat σ as the independent variable and to define

$$\hat{\theta}(\sigma) = \theta(t(\sigma)), \tag{2.8}$$

where $t(\sigma)$ is the inverse of $\sigma(t)$. The effect of the transformation (2.8) is that we now think of the orientation of the microstructure in a context where time does not appear explicitly. This transformation is well defined except at points where $\mathrm{d}\sigma/\mathrm{d}t = 0$, i.e. at fixed points of (2.7*a*); however, this limitation is not a problem as we shall see.

The transformation facilitates the qualitative analysis of (2.7*a*, *b*), in the following way. We can rewrite (2.7*b*) using (2.8) as

$$\dot{\theta}(t) = \hat{\theta}'(\sigma)\,\dot{\sigma}(t). \tag{2.9}$$

Hence substituting for $\mathrm{d}\sigma/\mathrm{d}t$ and $\mathrm{d}\theta/\mathrm{d}t$ from (2.7), we obtain

$$\hat{\theta}'(\sigma) = \frac{-\frac{1}{2}G(e\cos 2\sigma + \frac{1}{2}\gamma \sin 2\sigma)}{\frac{1}{2}\omega - Ge\sin 2\sigma + \frac{1}{2}G\gamma\cos 2\sigma}\sin 2\hat{\theta}. \tag{2.10}$$

Next we integrate this equation from $\sigma(0)$ to $\sigma(t)$:

$$\tfrac{1}{2}\log\frac{\tan\hat{\theta}(\sigma(t))}{\tan\hat{\theta}(\sigma(0))} = \tfrac{1}{4}\log\left[\frac{\frac{1}{2}\omega - Ge\sin 2\sigma(t) + \frac{1}{2}G\gamma\cos 2\sigma(t)}{\frac{1}{2}\omega - Ge\sin 2\sigma(0) + \frac{1}{2}G\gamma\cos 2\sigma(0)}\right],$$

and, upon simplification, this can be expressed in the form

$$\tan\hat{\theta}(\sigma(t)) = \tan\hat{\theta}(\sigma(0))\left[\frac{\dot{\sigma}(t)}{\dot{\sigma}(0)}\right]^{\frac{1}{2}}. \tag{2.11}$$

The interpretation of (2.11) is as follows. For a given initial condition $(\sigma(0), \theta(0))$, equation (2.11) describes a curve in (σ, θ)-space. Because the coordinates (σ, θ) are modified spherical polar coordinates, the trajectories (2.11) may be thought of as residing on the surface of a sphere. This sphere travels along with the centre of gravity of the microstructural element but does not rotate relative to the inertial coordinate system (x, y, z). Thus the curve (2.11) may be interpreted as the locus of the intersection of $\boldsymbol{R}$ with the spherical surface as the microstructure tumbles around in the flow.

Before we proceed, let us consider (2.7*a*). Recall that the transformation (2.8) is valid provided that $\mathrm{d}\sigma/\mathrm{d}t \neq 0$. From (2.7*a*), we deduce

$$\dot{\sigma} = 0 \Rightarrow \tan\sigma_{\pm}^{*} = \frac{-2Ge}{G\gamma-\omega} \pm \frac{(D)^{\frac{1}{2}}}{G\gamma-\omega}. \tag{2.12a}$$

Clearly, the existence of a fixed point where $\mathrm{d}\sigma/\mathrm{d}t = 0$ requires that the *discriminant*

$$D = 4G^2e^2 + G^2\gamma^2 - \omega^2 \tag{2.12b}$$

be positive or zero. One can see from (2.12) that the presence or absence of equilibrium orientations is a result of a competition between the rate-of-strain tensor that tends to produce a fixed orientation along the principal axis of strain and the vorticity that tends to cause the microstructure to rotate.

In the absence of vorticity, i.e. when $\omega = 0$, (2.12) implies that there will be two equilibrium orientations that coincide with the principal axes of the rate-of-strain tensor $\boldsymbol{E}$. Because the flow is assumed to be two-dimensional and incompressible, the trace of the rate-of-strain tensor must be zero. In other words, the two eigenvalues of the rate-of-strain tensor have opposite sign, corresponding to an outflow direction (+) and an inflow direction (−) relative to a coordinate system travelling with the microstructural element, as was shown in §2.1. As the microstructural element moves along in a flow with zero vorticity, it tends to align with the relative outflow direction, corresponding to the positive eigenvalue of the rate-of-strain tensor. In the opposite case, when $\boldsymbol{E} = 0$, and vorticity is non-zero, there are no equilibria and the microstructure simply rotates or tumbles in the flow. The relative importance of the rate of strain (e, γ) and the vorticity ω is signalled by the sign of the discriminant D: when $D < 0$, the microstructural element rotates; when $D \geqslant 0$, the microstructural element aligns in some direction.

For example, the case of uniform shear flow aligned with the x-axis has the flow parameters $e = 0$, $\gamma = -\omega = \lambda$. Thus when the shape factor $G < 1$, as is the case with most axisymmetric particles, the discriminant $D = (G^2-1)\lambda^2$ is negative and it can be seen from (2.12) that the microstructure simply rotates. On the other hand, Bretherton (1962) has shown that there are certain exotic types of microstructure with shape factor $G > 1$, and in this case it can be seen that there are two equilibrium orientations in uniform shear flow.

Bretherton also observed that microstructure with $G = 1$ rotates in uniform shear flow into alignment with the streamlines of the undisturbed flow. This corresponds to the degenerate case $D = 0$, in which the attracting and repelling equilibria ($D > 0$)

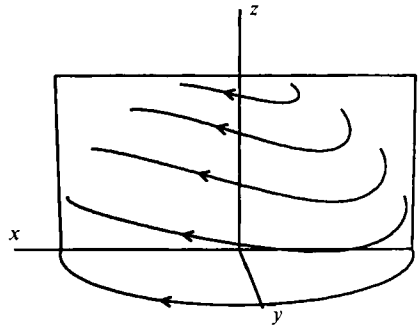

FIGURE 2. Integral curves of the two-dimensional simple-flow orientation problem with negative discriminant ($D < 0$). Here all trajectories are periodic; there are no attractors. Here we have taken the parameter values $e = 1$, $\gamma = 0$, $\omega = -4$ and $G = 1$. This corresponds to a flow with elliptical streamlines $\psi = xy + x^2 + y^2$.

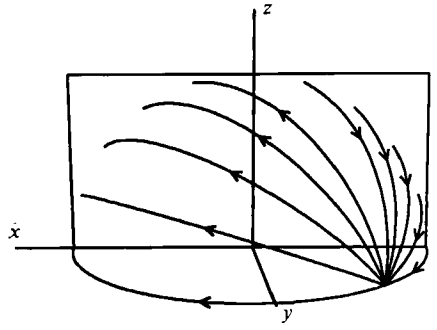

FIGURE 3. Integral curves of the two-dimensional simple-flow orientation problem with zero discriminant ($D = 0$). There is a single metastable equilibrium orientation. The relevant parameter values are $e = 2$, $\gamma = 0$, $\omega = -4$ and $G = 1$. This corresponds to a parallel flow with $\psi = 2xy + x^2 + y^2$.

coalesce to yield a single metastable equilibrium orientation. We remark that for any value of G it is possible to construct a flow that yields degenerate dynamics. To see this, consider a simple flow field $\psi = \frac{1}{2}ax^2 + \frac{1}{2}by^2$. One easily computes $e = 0$, $\gamma = b - a$ and $\omega = -a - b$. Thus for a given G, we have the degenerate case $D = 0$ when

$$a = \frac{(1-G^2)\,b}{(G^2-1)-(1+2G^2)\,b}.$$

For example, when $G = 1$, we obtain Bretherton's result $a = 0$ corresponding to uniform shear. However, when $G < 1$, the streamlines of the degenerate flow are hyperbolic with respect to non-rotating coordinates moving with the centre of mass of the microstructural element, and when $G > 1$ the streamlines are elliptic. As we shall see below, the degenerate case is important in understanding the robustness of the dynamics to changes in the model equations.

Now we return to the solution (2.11). With the information provided by the curves (2.11) it is a simple matter to draw the integral curves of (2.7*a*, *b*) when the flow parameters are constant. These pictures come in three varieties, examples of which are given in figures 2, 3 and 4. In these figures, we have plotted the solution over a quarter sphere $[0 \leqslant \sigma < \pi,\ 0 \leqslant \theta \leqslant \frac{1}{2}\pi]$. The fluid flows that correspond to the

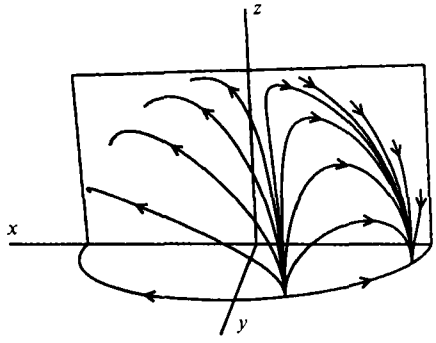

FIGURE 4. Integral curves of the two-dimensional simple-flow orientation problem with positive discriminant ($D > 0$). There are two equilibrium orientations, one stable and one unstable. The relevant parameter values are $e = 3$, $\gamma = 0$, $\omega = -4$ and $G = 1$. This corresponds to flow with hyperbolic streamlines $\psi = 3xy + x^2 + y^2$.

microstructure dynamics shown in figures 2, 3 and 4 are all simple (two-dimensional) flows with parameters $e = 1$, 2 and 3, respectively, and $\gamma = 0$, $\omega = -4$. The streamlines of the undisturbed flow fields are elliptical, parallel and hyperbolic, respectively.

The curves in figures 2–4 are to be interpreted as follows. A point on a curve gives the instantaneous orientation of the state vector of the microstructure relative to the inertial frame (x, y, z). Each curve in figures 2–4 represent a different set of initial conditions $(\sigma(0), \theta(0))$ that are seen to define uniquely the dynamics through (2.11). Curves based at different initial conditions intersect only at equilibrium orientations (singular points), when these exist. One can see from the figures that nearly all motions are three dimensional, by which we mean that nearly all motions are characterized by the state vector of the microstructure moving in or out of the plane of the flow. However, there are some motions that take place only in the plane of the flow.

In figure 2, because $D < 0$, there are no equilibrium orientations. In fact, one can see from (2.11) and (2.7a) that the state vector of the microstructure merely wobbles in a periodic fashion. This means that if $\theta = \frac{1}{4}\pi$ when $\sigma = 0$, say, θ will again be $\frac{1}{4}\pi$ when the state vector has rotated around so that σ is again 0 (or π, equivalently). In figure 3 we depict the degenerate case $D = 0$, where there is a single (metastable) equilibrium orientation. The equilibrium orientation is neither wholly stable nor unstable, as some neighbouring orientations are attracted while others are repelled. In figure 4, where $D > 0$, there is a single (stable) equilibrium orientation that all other orientations approach as time increases, and a second (unstable) equilibrium orientation that repels all other orientations. In such a situation, the state vector approaches the stable orientation and remains there for all time.

Of course, (2.11) provides no information on the speed with which a given trajectory in (σ, θ)-space is followed. However, it is an easy matter to integrate (2.7a) directly in the autonomous case, as we show below, and thus reconstruct $(\sigma(t), \theta(t))$ through (2.11).

Finally, we consider the stretch degree of freedom (ρ) for the simple flow case. As in (2.8) we define

$$\hat{\rho}(\sigma) = \rho(t(\sigma)), \tag{2.13}$$

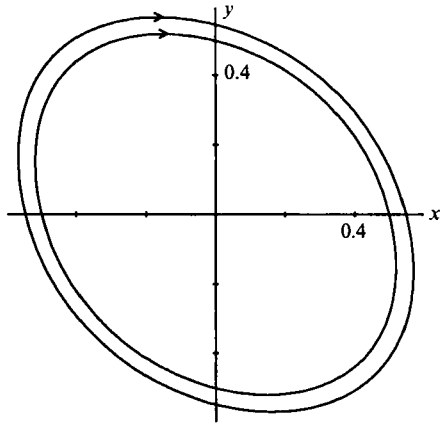

FIGURE 5. Integral curves of the orientation in the plane and stretch variables for the parameters of figure 2 and $F = 1$, $\alpha = 0$. Plotted is the coordinate of the tip of the state vector $\boldsymbol{R}$, $\rho(t)/\rho(0)$, as seen from the centroid of the microstructure for initial orientations $\sigma_0 = 0$ and $\frac{1}{3}\pi$.

where $\mathrm{d}\sigma/\mathrm{d}t \neq 0$. Equation (2.7*c*) can be rewritten as

$$\frac{\hat{\rho}'(\sigma)}{\hat{\rho}(\sigma)} = \left[\frac{-1}{F+1}\frac{1}{2}\frac{\mathrm{d}\dot{\sigma}}{\mathrm{d}\sigma}\cos^2\hat{\theta} - \frac{\alpha}{F+1}\right]\frac{1}{\dot{\sigma}}, \tag{2.14}$$

where we interpret $\mathrm{d}\sigma/\mathrm{d}t$ as a function of σ, given by (2.7*a*). The equation (2.14) can then be integrated using (2.11). The result is

$$\log\frac{\hat{\rho}(\sigma(t))}{\hat{\rho}(\sigma(0))} = \frac{-1}{F+1}\frac{1}{2}\log\left[\frac{\dot{\sigma}(t)}{\dot{\sigma}(0)}\left(\frac{\dot{\sigma}(0)+\dot{\sigma}(0)\tan^2\theta(0)}{\dot{\sigma}(0)+\dot{\sigma}(t)\tan^2\theta(0)}\right)^2\right] - \frac{\alpha}{F+1}I(\sigma(0),\sigma(t)). \tag{2.15a}$$

The form of the integral $I = \int \mathrm{d}\sigma/(\mathrm{d}\sigma/\mathrm{d}t) = t$ depends on the discriminant, as follows: when $D < 0$,

$$t = I(\sigma(0),\sigma(t)) = \frac{2}{(-D)^{\frac{1}{2}}}\tan^{-1}\left[\frac{-2Ge-(G\gamma-\omega)\tan\sigma}{(-D)^{\frac{1}{2}}}\right]_{\sigma-\sigma(0)}^{\sigma-\sigma(t)}; \tag{2.15b}$$

when $D = 0$,

$$t = I(\sigma(0),\sigma(t)) = \frac{1}{\omega}\left[\frac{+\omega+(2Ge-G\gamma)\cos 2\sigma+(2Ge+G\gamma)\sin 2\sigma}{+\omega+(2Ge+G\gamma)\cos 2\sigma-(2Ge-G\gamma)\sin 2\sigma}\right]_{\sigma-\sigma(0)}^{\sigma-\sigma(t)}; \tag{2.15c}$$

and when $D > 0$,

$$t = I(\sigma(0),\sigma(t)) = \frac{1}{D^{\frac{1}{2}}}\log\left[\frac{-2Ge-D^{\frac{1}{2}}-(G\gamma-\omega)\tan\sigma}{-2Ge+D^{\frac{1}{2}}-(G\gamma-\omega)\tan\sigma}\right]_{\sigma-\sigma(0)}^{\sigma-\sigma(t)}. \tag{2.15d}$$

Note that when $\omega = G\gamma$, special forms of (2.15*b–d*) apply.

In order to understand the solution (2.15), we show plots in figures 5–7 of the solution for the same values of the flow parameters used to generate the orientation curves of figures 2–4. For simplicity, we restrict the plots to those solutions with $\theta(0) = 0$. One can see from (2.1) that if $\theta(0) = 0$, then $\theta(t) = 0$ for all time; thus microstructural elements with directors parallel to the (x, y)-plane remain so. In each

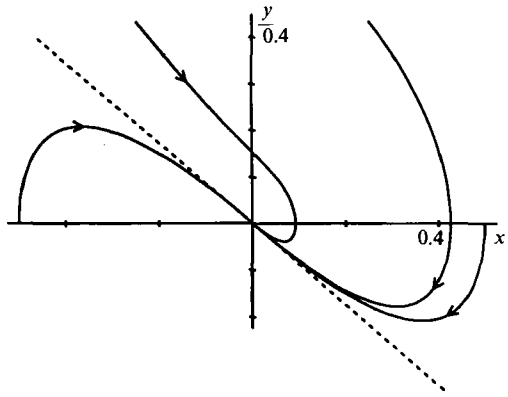

FIGURE 6. Integral curves of the orientation in the plane and stretch variables for the parameters of figure 3 and $F = 1$, $\alpha = 2$. Plotted is the coordinate of the tip of the state vector $\boldsymbol{R}$, $\rho(t)/\rho(0)$, as seen from the centroid for various initial orientations $\sigma_0 = 0$, $\frac{1}{3}\pi$, $\frac{2}{3}\pi$ and π. The dashed line represents the metastable orientation of figure 3.

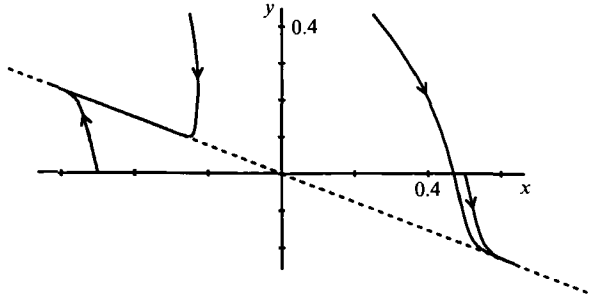

FIGURE 7. Integral curves of the orientation in the plane and stretch variables for the parameters of figure 4 and $F = 1$, $\alpha = 2$. Plotted is the coordinate of the tip of the state vector $\boldsymbol{R}$, $\rho(t)/\rho(0)$, as seen from the centroid for various initial orientations $\sigma_0 = 0$, $\frac{1}{3}\pi$, $\frac{2}{3}\pi$ and π. The microstructure stretches in an unbounded fashion as time increases. The dashed line represents the stable orientation of figure 4.

of the figures, the curves correspond to the locus of the tip of the state vector of the microstructure as seen from a coordinate system travelling with the centre of gravity of the microstructure. The orientation of this coordinate system relative to the inertial frame (x, y, z) is fixed. Different curves in the same figure correspond to different initial orientations in the plane. The initial condition for the length of the microstructure is $\rho(0) = 1$; equivalently, figures 5–7 may be interpreted as plots of $\rho(t)/\rho(0)$ versus $\sigma(t)$. Again, it is important to keep in mind that $\theta = 0$ in the solutions of figures 5–7.

In figure 5 we show the stretch history for the flow parameters of figure 2 with the spring constant $\alpha = 0$. In this case, the discriminant $D < 0$ and the stretch history is periodic in σ; consequently, it is also periodic in time. Note that if we chose $\alpha > 0$, the length of the microstructure would have approached zero for large times.

In figure 6 we show the stretch history for the flow parameters of figure 3 with the spring constant $\alpha = 2$. Recall that this is the degenerate case with discriminant $D = 0$. One can see that as the microstructure assumes the metastable orientation, the state vector contracts under the action of the spring. The metastable orientation of

figure 3 is presented by the dashed line in figure 6. As time tends to infinity, the model breaks down because the microstructure contracts to a point.

In figure 7 we show the stretch history for the flow parameters of figure 4 with the spring constant $\alpha = 2$. Here, the discriminant $D > 0$ and the microstructure quickly moves to the stable orientation. The stable orientation in figure 4 is represented by the dashed line in figure 7. The flow in this case is sufficiently strongly stretching that the state vector lengthens despite the spring constant $\alpha = 2$. As time tends to infinity, the model breaks down because the microstructure extends without bound.

Olbricht *et al.* (1982) derive a sufficient condition (known as the strong-flow criterion) for stretching to occur in simple flows, namely

$$D^{\frac{1}{2}} > 2\alpha. \tag{2.16}$$

This criterion is satisfied in the example of figure 7. One may obtain this criterion by integrating (2.7*c*) at the equilibrium orientation $(\sigma, \theta) = (\sigma_+^*, 0)$; this yields

$$\frac{\rho}{\rho_0} = \exp\left(\frac{t}{1+F}(\tfrac{1}{2}D^{\frac{1}{2}} - \alpha)\right).$$

We see that the strong-flow criterion (2.16) is a sufficient condition for stretch at the (constant) equilibrium orientation $(\sigma, \theta) = (\sigma_+^*, 0)$. This orientation corresponds to an eigenvector of the velocity gradient tensor in the case $G = 1$, and $\frac{1}{2}D^{\frac{1}{2}}$ is the corresponding eigenvalue.

This ends our review of the orientation and stretch of microstructural elements for simple two-dimensional flows. Because the flow parameters e, γ and ω are constants in this case, the system (2.7) is autonomous, and this has permitted us to find the equilibrium orientations (2.12) and to transform the equations via (2.8) and (2.13). The resulting forms proved to be integrable. As we shall see below, the dynamics of microstructure in complex flows are much more interesting.

A remark about the difference between simple and complex flows is in order. It is tempting to analyse the dynamics of microstructure in complex flows in the following way. Because such flows are unsteady in the Lagrangian frame, the flow parameters e, γ and ω change with time. One might attempt (incorrectly) to analyse the attraction or repulsion of the instantaneous orientation $(\sigma = \sigma_\pm^*(t), \theta = 0)$ given by (2.12). This would be incorrect as we demonstrate by example in §3.1, below. The reason is that $(\sigma = \sigma_\pm^*, \theta = 0)$ is not an integral curve of the system (2.7) for complex flows, in general. We must develop other techniques for the analysis of microstructure in complex flows.

For the subsequent discussion, it is sufficient to remember that if D is strictly positive, there are two equilibria σ_+^* and σ_-^* in $[0, \pi)$, one of which is linearly stable and the other is linearly unstable. If $D = 0$, there is a single degenerate (metastable) equilibrium and if $D < 0$ there are no equilibria.

2.3. *Robustness of the model in simple flows*

In the final analysis, any investigation of the dynamics of microstructure suspended in fluid flows must make certain simplifying assumptions in order to achieve a tractable problem. The results of such an investigation are valuable only to the extent that they are not obviated by the small differences between the analytical problem and the real, physical system. In other words, one must be concerned with the sensitivity of the dynamics to small changes in the model equations.

Implicit in the equation (2.1) is the assumption that the microstructure is sufficiently small that the dynamics depend only on the velocity gradient tensor of

the surrounding flow and not on higher-order derivatives of the velocity. We could imagine that for larger microstructural elements this would not be the case. A second important assumption is the restriction to two-dimensional flows. It is important to establish that the result of the analysis of §2.2 would not change radically if either of these assumptions were to be relaxed slightly. Moreover, we would like to be certain that small diffusive effects would not radically alter our results.

These are questions about the structural stability of the system (2.7) to perturbations that include small diffusion, slight three-dimensionality or slightly more complicated dependence of the dynamics on the fluid flow. A resumé of the mathematical results concerning the structural stability of various classes of systems of differential equations can be found in Arnol'd (1983). The answer to the question of structural stability depends in a complicated way on the topology of the space in which the vector field of a given system of differential equations resides (e.g. circle, torus, sphere, etc.), and on the solutions of the given system.

In this subsection, we shall consider the structural stability of the system (2.7) in the case where the flow parameters e, γ and ω are constant in time, that is to say for simple flows. Later, we shall consider the robustness of the model in the case of complex flows. For simple flows, we can make use of the results in Arnol'd (1983) to deduce that a perturbation to the model equations can change the qualitative nature of solutions when $D < 0$ or $D = 0$, but that such a perturbation will leave the case $D > 0$ (qualitatively) unchanged. To understand this result from a physical point of view, we examine each case in turn.

As shown in §2.2, when $D < 0$ all orientation time traces are closed (periodic) curves. A small perturbation such as Brownian diffusion, say, would destroy this structure of the solution and thus orientation time-traces would no longer be periodic. This constitutes a qualitative change in the solutions of the system in response to the perturbation, and so we say that the model equations are structurally unstable in the case $D < 0$. In other words an $O(\epsilon)$ change in the model equations can lead to an $O(1)$ change in the solutions, possibly over a long time. The effect of weak Brownian rotation on the orientation of rigid spheroids in uniform shear flow was investigated by Leal & Hinch (1971). Another manifestation of the structural instability of the system when $D < 0$ was noted in Olbricht *et al.* (1982); predominantly two-dimensional flows with $D < 0$, and sufficiently large norm of the velocity gradient tensor are strong flows if there is slight three-dimensionality.

In the degenerate case $D = 0$, there is a single metastable equilibrium orientation. This equilibrium orientation is metastable because the eigenvalues of the system (2.7) linearized about the equilibrium orientation have zero real part. A change in the model equations corresponding to slight three-dimensionality, say, could change the metastable equilibrium to either a stable–unstable pair of equilibria, or cause it to disappear altogether. Thus the system (2.7) is structurally unstable in the degenerate case $D = 0$, also.

The only structurally stable situation is the case $D > 0$. There are no closed orientation solutions in this case, and all singular points are either wholly stable or wholly unstable. The solutions for $D > 0$ will not change much if the model is altered slightly to account for Brownian motion, three-dimensional effects, etc. The dynamics in the simple flow case $D > 0$ are robust.

3. The dynamics of microstructure in complex flows

The most fruitful way of untangling the motions of a dynamical system is often to look for attractors. In the autonomous case of (2.7), the attractor consists of a single orientation in the plane of the flow when the discriminant is positive. When the discriminant is negative, there is no attractor. When the discriminant is zero, there is a single, metastable equilibrium orientation in the plane of the flow.

In non-autonomous systems, attractors are normally more complicated than a simple fixed point. Generally, we seek an integral curve, or solution of the differential equations, to which other integral curves are attracted over some interval of time. For simplicity, we shall first examine the planar orientation problem (σ) since (2.7a) decouples from (2.7b, c). In some respects, our methods are related to conventional dynamical stability analysis. A brief discussion of this point is given in the Appendix. Before beginning the detailed analysis, perhaps it is useful to recall some facts about non-autonomous differential equations.

3.1. *Distinguishing aspects of non-autonomous differential equations*

In order to illustrate some of the differences between autonomous and non-autonomous differential equations, we review some basic principles that serve to distinguish the two classes of systems.

PRINCIPLE 1. *Solutions of the equation* $\mathrm{d}x/\mathrm{d}t = f(x,t) = 0$ *with time 'frozen', i.e. considered as a parameter, are not solutions of* $\mathrm{d}x/\mathrm{d}t = f(x,t)$, *in general. The attractors one finds for the system* $\mathrm{d}x/\mathrm{d}t = f(x,t)$ *at a fixed instant of time are not generally solutions of the time dependent system.*

PRINCIPLE 2. *The stability problem for a time-dependent integral curve cannot be approached by a standard linear stability analysis, i.e. by analysing the eigenvalues of the linearization of the disturbance evolution equations.*

PRINCIPLE 3. *Integral curves of differential equations that are autonomous except for a slow time-dependent term can be qualitatively different in a global sense from the integral curves arising from the autonomous part alone.*

These principles may be elementary to some readers of the present paper. However, we shall demonstrate each principle in turn with an example for those who may not be so familiar with non-autonomous systems.

Illustration of Principle 1

We consider the non-autonomous equation

$$\dot{x}(t) = -(x-t),$$

where x is real and $t > 0$. As an illustration of Principle 1, we set $\mathrm{d}x/\mathrm{d}t = 0$ and search for an attractor. This (incorrect) procedure would yield $x = t$ as the 'solution' to $\mathrm{d}x/\mathrm{d}t = 0$; a stability analysis would then reveal that $x = t$ is a global attractor. This procedure is incorrect, however, because $x = t$ is not a solution to the original differential equation, as we now show. We can integrate the time-dependent equation to obtain the solution

$$x(t) = t-1+\mathrm{e}^{-t}(1+x_0),$$

which depends on the initial condition x_0. Note that all integral curves $x(t)$ quickly approach the curve $x = t-1$ at large times. Thus $x = t-1$, which is itself an integral

curve with initial condition $x_0 = -1$, attracts all other integral curves. Thus the solutions of the 'frozen time' equations $dx/dt = 0$ have nothing whatsoever to do with the attractors of the corresponding non-autonomous system.

In our analysis of microstructure in complex flows, Principle 1 reveals that attractors for the orientation dynamics are not simply given by $(\sigma = \sigma_{\pm}^{*}(t),\ \theta = 0)$ (see equation (2.12)) evaluated at an instant of time t. Thus the strong-flow criterion for simple flows, which relies on the fact that $(\sigma = \sigma_{+}^{*},\ \theta = 0)$ is a solution of (2.7), cannot apply to general complex flows.

Illustration of Principle 2

The second example is due to Markus & Yamabe (1960) and is discussed by Hale (1969). We consider a two-dimensional, non-autonomous (linear) system of equations for $x = (x_1, x_2)$,

$$\frac{dx}{dt} = A(t)\,x, \quad A(t) = \begin{bmatrix} -1+\frac{3}{2}\cos^2 t & 1-\frac{3}{2}\sin t\cos t \\ -1-\frac{3}{2}\sin t\cos t & -1+\frac{3}{2}\sin^2 t \end{bmatrix}.$$

A standard linear stability analysis of the equilibrium $(x_1, x_2) = (0, 0)$ would proceed by analysing the eigenvalues of the disturbance evolution equations $dx/dt = A(t)\,x$. The eigenvalues of the time dependent matrix $A(t)$ are the constants

$$\lambda = \frac{-1}{4} \pm \frac{i7^{\frac{1}{2}}}{4},$$

which *both* have negative real parts. It would thus seem that the origin $x = 0$ is stable for this linear system. However, one solution of the time-dependent equation is

$$x = e^{\frac{1}{2}t}\begin{pmatrix} -\cos t \\ \sin t \end{pmatrix},$$

which is unbounded for large times. Because the original equation is linear, any general solution must contain this unbounded solution. Thus one cannot test for stability in non-autonomous equations by examining the eigenvalues of the (time-dependent) matrix associated with the linearized equations; one must instead examine the solution of these equations.

Illustration of Principle 3

Principle 3 concerns differential equations with slow-time-dependent forcing. One example is

$$\dot{\sigma} = \sin 2\sigma \cos \epsilon t,$$

which has the solution

$$\sigma(t) = \tan^{-1}\left[\exp\left(\frac{2}{\epsilon}\sin \epsilon t\right)\tan \sigma_0\right],$$

when $\epsilon > 0$. When $\epsilon > 0$, one observes that every integral curve is periodic with period $T = 2\pi/\epsilon$.

When $\epsilon = 0$, however, the example equation is autonomous, with solution

$$\sigma_{\epsilon=0}(t) = \tan^{-1}[e^{2t}\tan \sigma_0].$$

Thus when $\epsilon = 0$, every integral curve tends to $\sigma = \frac{1}{2}\pi$. Despite the fact that we can choose $\epsilon > 0$ as small as we like, there are important global differences in the

solutions of the autonomous ($\epsilon = 0$) and non-autonomous ($\epsilon > 0$) equations when $t = O(\epsilon^{-1})$ or larger.

A related example that serves to illustrate Principle 3 is the system

$$\dot{x} = \frac{\partial \psi}{\partial y}(x, y, \lambda),$$

$$\dot{y} = -\frac{\partial \psi}{\partial x}(x, y, \lambda),$$

$$\dot{\lambda} = \epsilon,$$

which might be a system of equations for the particle paths in a fluid flow where the stream function ψ depends on a slowly varying parameter λ (for $\epsilon > 0$). When $\epsilon = 0$, the particle paths are level curves of the stream function, thus we say that the motion is integrable. When $\epsilon > 0$, no matter how small, the particle paths no longer coincide with level curves of the stream function, in general. In fact, for particular stream functions, it is well known that the particle paths may be chaotic when $\epsilon > 0$. This latter statement means that the particle paths depend so sensitively on their initial position that one could not possibly predict the motion forever with only a finite accuracy in measurement of the initial position. This could be true despite the fact that the equations are deterministic. This phenomenon is the subject of a wealth of references on chaotic advection, or Lagrangian turbulence, as it is sometimes called, including Aref (1984), Holmes (1984), Chaiken *et al.* (1986), and Kaper & Wiggins (1989), among others.

With the three Principles in mind, let us return to the flow-microstructure problem, which is governed by the set of equations (2.7), but with the flow parameters now regarded as functions of time rather than constants. We remark that in the case $G = 1$, where the microstructure has the same dynamic response as a line element of the fluid, the discriminant D is four times the 'persistence of strain' squared, that was recently proposed by Dresselhaus & Tabor (1989) as a means to characterize quite general dynamical systems based on the geometry of their attracting sets. When applied to flow-microstructure systems, Dresselhaus & Tabor show that the value of the persistence of strain is related to the folding and stretching of line elements of the fluid owing to the flow. However, this analysis depends on the eigenvalues of the disturbance evolution equation linearized about an attracting set of interest. In the fluid problems they consider, the attracting sets correspond to particle paths in the flow. As we have demonstrated, however, when the linearized disturbance evolution equation is time dependent, the instantaneous eigenvalues do not capture the dynamical behaviour near the attracting set. For this reason, it is clear that the persistence of strain concept would not generally be useful in problems where the linearized disturbance evolution equation are time dependent. For our particular application, this corresponds to the fact that we cannot base the analysis of stretching and orientation of microstructure simply on the instantaneous eigenvalues of 'equilibrium' orientations when those 'equilibrium' orientations are themselves time dependent, as they are in complex flows.

3.2. *The orientation problem in the plane of the flow*

Now we move on to the analysis of microstructure suspended in complex flows. Our goal in §§3.2 and 3.3 is to develop an understanding of orientation dynamics of the microstructure, and to develop a strong-flow criterion that may be applied to microstructure in complex flows.

We are interested in finding an integral curve $\sigma(t)$ of (2.7*a*) to which other integral curves are attracted over the time interval $[0, T]$, say. Principle 1 of §3.1 reveals that we cannot find such an attractor as we did in the case of simple flows in §2.2. Principle 2 cautions that we cannot identify whether or not an integral curve is an attractor by a standard linear stability analysis. Therefore, we must develop new techniques as we go along. Our approach to this problem is to consider the difference between two orientations at an instant of time

$$\delta(t) \equiv \sigma_1(t) - \sigma_2(t), \tag{3.1}$$

where $\sigma_1(t)$ and $\sigma_2(t)$ are two integral curves of (2.7*a*) with time-dependent flow parameters. We can obtain an evolution equation for $\delta(t)$ by differentiating (3.1) and using (2.7*a*):

$$\begin{aligned}\dot{\delta}(t) &\equiv \dot{\sigma}_1(t) - \dot{\sigma}_2(t) \\ &= [\tfrac{1}{2}\omega - Ge \sin 2\sigma_1 + \tfrac{1}{2}G\gamma \cos 2\sigma_1] - [\tfrac{1}{2}\omega - Ge \sin 2\sigma_2 + \tfrac{1}{2}G\gamma \cos 2\sigma_2].\end{aligned} \tag{3.2}$$

Next, we use various trigonometric identities to rewrite (3.2) as

$$\dot{\delta} = -[2Ge \cos(\sigma_1 + \sigma_2) + G\gamma \sin(\sigma_1 + \sigma_2)] \sin \delta. \tag{3.3}$$

Now, because the sum of σ_1 and σ_2 is independent from the difference of σ_1 and σ_2, we can integrate (3.3) formally to obtain

$$\log\left[\frac{\tan \frac{1}{2}\delta(T)}{\tan \frac{1}{2}\delta(0)}\right] = -\int_0^T [2Ge(t) \cos(\sigma_1(t) + \sigma_2(t)) + G\gamma(t) \sin(\sigma_1(t) + \sigma_2(t))] \, \mathrm{d}t. \tag{3.4}$$

We refer to the integral on the right-hand side of (3.4) as the contraction exponent of the integral curves $\sigma_1(t)$ and $\sigma_2(t)$ over [0, T], or simply the contraction exponent (CE):

$$\mathrm{CE}[\sigma_1(0), \sigma_2(0); T] \equiv \int_0^T [2Ge(t) \cos(\sigma_1(t) + \sigma_2(t)) + G\gamma(t) \sin(\sigma_1(t) + \sigma_2(t))] \, \mathrm{d}t. \tag{3.5}$$

Note that the CE depends on the initial conditions $\sigma_1(0)$ and $\sigma_2(0)$ rather than the entire integral curves ($\sigma_1(t)$ and $\sigma_2(t)$, $0 \leqslant t \leqslant T$) because the integral curves are uniquely determined by their initial conditions. The term contraction exponent is motivated by rearranging (3.4) to read

$$\tan \tfrac{1}{2}\delta(T) = \exp[-\mathrm{CE}[\sigma_1(0), \sigma_2(0); T]] \tan \tfrac{1}{2}\delta(0). \tag{3.6}$$

Bearing in mind that the tangent function is monotonic, one can see that the difference between two integral curves δ is less at time T than at time 0 if and only if the contraction exponent is positive. Thus the contraction exponent quantifies the notion of attraction for the non-autonomous orientation problem in the plane of the flow.

In passing, we remark that (3.6) is a discrete time map corresponding to the differential equation (3.3). This means that one application of the discrete time map (which maps $\delta(0)$ to $\delta(T)$) is exactly equivalent to integrating the related differential equation forward in time over the interval $0 \leqslant t \leqslant T$.

If we are interested in whether or not a particular integral curve attracts nearby integral curves, we can specialize the contraction exponent as follows. Let $\sigma(t)$ be an integral curve, and $\sigma(t) + \epsilon(t)$, be a nearby integral curve. Then we have

$$\mathrm{CE}[\sigma(0), \sigma(0) + \epsilon(0); T] = \mathrm{CE}[\sigma(0), \sigma(0); T] + O(|\epsilon(t)|). \tag{3.7}$$

We define the *nearby contraction exponent* to be

$$\frac{\mathrm{nCE}\,[\sigma(0);T]}{T} \equiv \frac{\mathrm{CE}\,[\sigma(0),\sigma(0);T]}{T}, \tag{3.8}$$

and from (3.6), we obtain an infinitesimal version of the discrete time map of the difference of the two integral curves:

$$\epsilon(T) = \epsilon(0)\exp\left(-\mathrm{nCE}\,[\sigma(0);T]\right), \tag{3.9}$$

which is valid provided that $\mathrm{nCE}\,[\sigma(0);T]$ is non-zero. Equation (3.9) is equivalent to the solution of the linearized disturbance evolution equation about the integral curve $\sigma(t;\sigma(0))$. Basing our stability characterization of $\sigma(t;\sigma(0))$ on (3.9) avoids the pathological situation pointed out in Principle 2 of §3.1.

In this section, we developed the contraction exponent to describe the attraction or repulsion of a particular integral curve $\sigma(t)$ for neighbouring integral curves. However, the nearby contraction exponent has other important uses, as we shall see below.

3.3. *The full dynamical problem for complex flows*

In the previous section, we were able to quantify the behaviour for the orientation problem in the plane of the flow by means of the contraction exponent. To be specific, if the contraction exponent for two distinct integral curves is positive (negative), the integral curves experience a net convergence (divergence) over the indicated time interval. In the neighbourhood of an integral curve, it is sufficient to examine the nearby contraction exponent in order to determine whether the integral curve is attracting its neighbours.

Now we move on to consider the out-of-plane and stretching degrees of freedom of the microstructure. We shall see that the nearby contraction exponent also gives information about these aspects of the dynamics. First, we consider (2.7*b*). We divide through by $\sin 2\theta$ and integrate from 0 to T:

$$\int_{\theta(0)}^{\theta(T)} \frac{\mathrm{d}\theta}{\sin 2\theta} = -\frac{1}{4}\int_0^T (2Ge\cos 2\sigma + G\gamma \sin 2\sigma)\,\mathrm{d}t. \tag{3.10}$$

Note that the right-hand side of (3.10) is just a constant multiplied by the nearby contraction exponent for the integral curve $\sigma(t)$ with initial condition $\sigma(0)$. Thus we obtain the discrete time map for the θ coordinate as

$$\tan\theta(T) = \exp\left[-\tfrac{1}{2}\mathrm{nCE}\,[\sigma(0);T]\right]\tan\theta(0). \tag{3.11}$$

Interpreting this result, we find that along attracting integral curves $\sigma(t)$, on which $\mathrm{nCE}\,[\sigma(0);T] > 0$, the state vector of the microstructure moves toward the plane of the flow.

Next we perform a similar integration of the stretch equation (2.7*c*). We divide (2.7*c*) by ρ and integrate using (3.11) to obtain the discrete time map for ρ:

$$\rho(T) = \rho(0)\left(\frac{1+\mathrm{e}^{-\mathrm{nCE}\,[\sigma(0);T]}\tan^2\theta(0)}{1+\tan^2\theta(0)}\right)^{1/2(F+1)} \exp\left[\frac{T}{F+1}\left(\frac{1}{2}\frac{\mathrm{nCE}\,[\sigma(0);T]}{T}-\alpha\right)\right]. \tag{3.12}$$

Thus along integral curves $\sigma(t)$ that are sufficiently strongly attracting, the microstructure will undergo an increase in length. By sufficient attraction, we mean

$$\max_{\sigma(0)}\left[\frac{\mathrm{nCE}\,[\sigma(0);T]}{T}-2\alpha\right] > 0. \tag{3.13}$$

The inequality (3.13) is therefore a (history dependent) strong-flow criterion for the stretch of microstructure in a complex two-dimensional flow. Equation (3.13) is a necessary and sufficient condition for stretch of an element of the microstructure over the time interval for some initial orientation. Note that the history-dependent strong-flow criterion (3.13) is based on an actual integral curve of the non-autonomous equations. Because (3.13) is derived from the solution $\rho(t)$ over a time interval, we have avoided the pathological situation pointed out in Principle 2 of §3.1.

We remark that if the system (2.7) is autonomous, then (3.13) evaluated on $\sigma(0) = \sigma_+^*$ (equation (2.12*a*)) gives the simple strong-flow criterion (2.16). Note, however, that the simple strong-flow criterion (2.16) cannot be applied to complex flows for two reasons: (i) it is based on the assumption that $(\sigma_+^*, 0)$ is a solution of the orientation dynamics, which is only true in a simple flow with $D \geqslant 0$, and (ii) it is based on a linear stability analysis. Thus, the incorrect use of the simple strong-flow criterion in complex flows violates Principles 1 and 2 of §3.1. In other words, the simple strong-flow criterion cannot be used in complex flows because it fails to take the history of the microstructure into account. The analysis leading to (3.13) shows the correct way in which to account for history, In §5, we give examples that demonstrate these ideas.

To utilize the results of this section, one would normally integrate (2.7*a*) for the complete set of possible initial conditions $\sigma(0)$ in $[0, \pi)$ over the time interval $[0, T]$ of interest. Next one computes $\mathrm{nCE}[\sigma(0); T]$ for each integral curve. This gives information about which integral curves are attracting, the power of that attraction, and also the discrete time map for the out-of-plane and stretching degrees of freedom.

We emphasize that the history-dependent strong-flow criterion is applicable to all unsteady, spatially inhomogeneous, two-dimensional flows. Before proceeding to the examples in §5, we derive some strong results concerning the orientation dynamics and stretching of microstructure in time-periodic flows.

4. Time-periodic flows

In this section we derive additional results that apply in the special case when the flow parameters ϵ, γ and ω are periodic functions of time, i.e. when the history of the microstructure is time-periodic. This important case arises when, for example, the particle path through a steady flow is periodic (recirculating), or when the stream function of a spatially homogeneous flow varies periodically in time. This situation is also important because we can make use of some powerful ideas from dynamical systems theory, such as the Poincaré map.

The additional results we derive in the case of time periodic flows consist of information about the orientation dynamics of elements of microstructure. Just as in simple flows, where there may be a (fixed) attracting equilibrium orientation, we show that in time periodic flows there may be a time periodic, globally attracting orientation. In §4.1, we show how to go about finding this attractor, and we demonstrate the connection between the presence of an attractor in the orientation dynamics and the stretch of an element of the microstructure. In §4.2, we discuss the robustness of our results concerning time periodic flows to perturbations of the model equations.

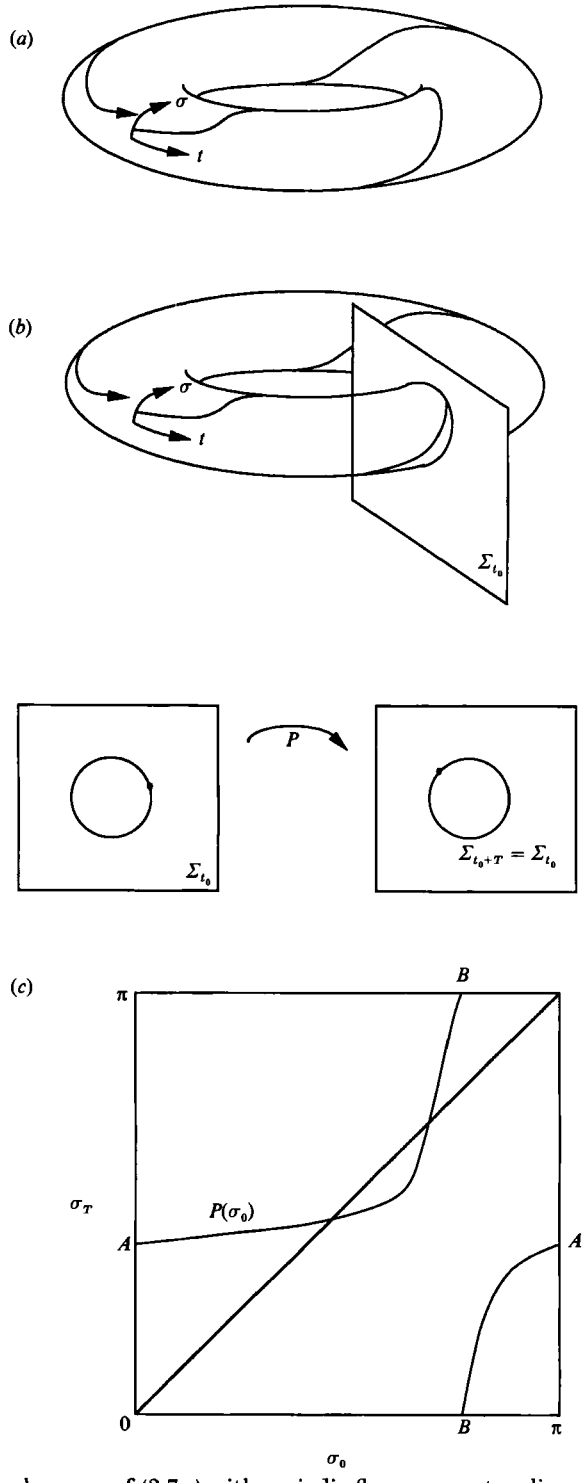

FIGURE 8. (*a*) Integral curves of (2.7*a*) with periodic flow parameters lie on the surface of a torus. (*b*) Geometric construction of the Poincaré map of (2.7*a*) with periodic flow parameters. (*c*) The form of the Poincaré map of (2.7*a*) with periodic flow parameters. The line $\sigma_T = \sigma_0$ is drawn for reference.

4.1. *The Poincaré map*

When the parameters ϵ, γ and ω are periodic functions of time, the vector field that describes the evolution of the conformation is also periodic in time, as can be seen from (2.7). By knowing how each conformation evolves over one period of the flow parameters, we know how any conformation evolves for all time, simply by stringing together the appropriate conformation changes over each period. This is the idea behind the Poincaré map, which is a discrete time map for a differential equation with periodic forcing just as (3.6) is a discrete time map corresponding to the differential equation (3.3). Thus, the Poincaré map is just a function that is exactly equivalent to integrating the differential evolution equations forward for one period of the flow parameters, starting from any arbitrary conformation as the initial condition. It is easy to see that a fixed point of k (integer) applications of the Poincaré map corresponds to a periodic integral curve of the differential equations with a period that is k times the period of the flow parameters. For background information on these ideas, see Guckenheimer & Holmes (1983), Wiggins (1988), or Arnol'd (1983).

We have, in fact, already computed the components of the Poincaré map in the θ- and ρ-directions; these are equations (3.11) and (3.12), respectively, where T is now to be interpreted as the period of the flow parameters. This leaves the Poincaré map for the orientation in the plane, σ, which we now consider. The principal important fact that we exploit is that the vector field of the differential equation (2.7*a*) is periodic in the angle σ and in time t. Just as the angles σ and $\sigma + k\pi$ are equivalent, for integer k, we also have equivalence of times t and $t + kT$, where T is the period of e, γ and ω. In other words the integral curves of (2.7*a*) with periodic flow parameters lie on the surface of a torus (or doughnut shape), which has coordinates σ around one circular generator and t around the perpendicular circular generator; see figure 8(*a*).

Now, the Poincaré map for σ is a discrete time map corresponding to the integration of (2.7*a*) forward in time over the interval $[0, T]$. Geometrically, we can think of the Poincaré map as follows. If we take a t = constant slice of the torus in figure 8(*a*), or mathematically if we define the cross-section

$$\Sigma_{t_0} = \{(t, \sigma) : t = t_0 + kT \quad (k = 0, 1, 2, 3, \ldots)\},$$

then the Poincaré map is a map from the cross-section to itself, as shown in figure 8(*b*). Thus if we apply the Poincaré map once to an initial point $\sigma(t_0)$, we obtain the intersection of the integral curve rooted at that initial point with the cross-section of the torus at time $t = t_0 + T$. Because the integral curves lie on the surface of a torus, the time $t_0 + T$ is identified with (or is equivalent to) t_0.

Owing to the absence of singular points in the vector field of (2.7*a*) on the torus, integral curves of (2.7*a*) cannot cross one another. Thus the Poincaré map preserves orientation (or cyclic ordering) on the circle. Moreover, the map is one to one, onto and differentiable with differentiable inverse. (In the compact language of dynamical systems, the Poincaré map is an orientation-preserving diffeomorphism of the circle. There is a great deal that is known about such maps, a resumé of which can be found in Guckenheimer & Holmes (1983).)

A fixed point of a Poincaré map corresponds to a periodic integral curve of the original differential equation. Furthermore, for Poincaré maps such as ours, it is known that if there is a fixed point then all initial conditions are asymptotically periodic. This latter statement means that any orientation integral curve that begins at an arbitrary initial orientation will eventually be attracted to the periodic integral curve that corresponds to the stable fixed point of the Poincaré map. Conversely, if

there are no points of period $m \geqslant 1$, then there are only complicated non-periodic orbits in the family of solutions to the underlying differential equation, some of which are dense in the circle.

Physically, periodic integral curves of the orientation have a special meaning. In the case where the fluid flow is recirculating (which gives rise to flow parameters of period T; see §5) a periodic integral curve of the orientation of period T is equivalent to a steady orientation in an Eulerian sense. In other words, if the orientation of the particles is periodic with the same period as the time it takes for the microstructure to return to the same spatial location, the orientation of the microstructure will appear to be constant in a laboratory reference. Thus finding periodic integral curves will be of critical importance in applications.

In what follows in the remainder of this section, we attempt to obtain as much qualitative information as we can about the Poincaré map for σ without actually computing it. Although we have not computed the Poincaré map for σ, as we have done for θ and ρ, we have computed its derivative, as stated in the following:

PROPOSITION. *Let P be the Poincaré map of equation (2.7a) with periodic flow parameters. In particular, let $P(\sigma_0) = \sigma_T$, where σ_T is the value of σ obtained by integrating*

$$\dot{\sigma} = \tfrac{1}{2}\omega - Ge \sin 2\sigma + \tfrac{1}{2}G\gamma \cos 2\sigma$$

forward in time over the period $[0, T]$ of the flow parameters, taking σ_0 as the initial condition. Then

$$\frac{\mathrm{d}P}{\mathrm{d}\sigma_0} = \exp(-\mathrm{nCE}[\sigma_0; T]). \tag{4.1}$$

Actually, we have already proved this proposition in deriving (3.9). Note that (4.1) applies to any σ_0, not just to a fixed point of the Poincaré map.

The importance piece of information one can glean from (4.1) is that the Poincaré map always has a positive derivative because the exponential of a finite quantity is never negative or zero. Now we will use this fact, and the fact that the map must be one-to-one to arrive at a qualitative picture of the Poincaré map.

We can integrate (4.1) with respect to σ_0 in order to obtain an expression for the Poincaré map itself. This expression is

$$P(\sigma_0) = \int_0^{\sigma_0} \mathrm{e}^{-\mathrm{nCE}[\lambda; T]}\,\mathrm{d}\lambda + P(0). \tag{4.2}$$

Here $P(0)$ is the Poincaré map of the origin, a constant. We chose to perform a definite integration of (4.1) starting from 0; we could have based the integration at a different point, however.

Next we must pay attention to the fact that the coordinate σ is periodic with period π. In other words, the values $\sigma = 0$ and $\sigma = \pi$ are equivalent, or identified. In fact, we can add an integral multiple of π to any value of σ and obtain an equivalent angle of the microstructure. Because this is true, it must also be true that the initial orientations $\sigma = 0$ and $\sigma = \pi$, which are equivalent, must map to the same final orientations, possibly with an additive factor of an integral multiple of π. Thus we have established the relation

$$P(\pi) = P(0) + k\pi, \tag{4.3}$$

where k is an integer. From the integral form of the Poincaré map, (4.2), this yields

$$\int_0^{\pi} \mathrm{e}^{-\mathrm{nCE}[\lambda; T]}\,\mathrm{d}\lambda = k\pi. \tag{4.4}$$

We can rule out the possibilities $k = 0$ and $k < 0$ because $e^x > 0$ for all x. Also, we can rule out the possibilities $k \geqslant 2$, because these values of k imply that the Poincaré map is multi-valued over the domain $0 \leqslant \sigma_0 < \pi$ and hence not invertible. Thus we are left with the result

$$\int_0^{\pi} e^{-nCE[\lambda;T]} d\lambda = \pi. \tag{4.5}$$

This result, coupled with (4.3), implies that the Poincaré map takes values over the range $P(0) \leqslant P(\sigma_0) < P(0)+\pi$ over its domain $0 \leqslant \sigma_0 < \pi$.

Now we have enough information to draw a qualitative picture of the Poincaré map. We know that the map always has positive slope. From (4.1), we observe that for σ_0 such that $nCE[\sigma_0; T] > 0$, the Poincaré map is relatively flat. Where $nCE[\sigma_0; T] < 0$, the Poincaré map is relatively steep. Also we know that the images of the points $\sigma_0 = 0$ and π differ by π. With this in mind, the Poincaré map must appear qualitatively like the sketch in figure 8(*c*). This picture is drawn in a standard way, in which no distinction is made between the equivalent angles $\sigma = \alpha + \pi$ where $0 \leqslant \alpha < \pi$, and $\sigma = \alpha$. For this reason, the images of the points 0 and π are equal, and the graph runs off the top of the page and jumps back onto the bottom.

We can identify non-degenerate fixed points as transverse intersections of the Poincaré map with the line $\sigma_T = \sigma_0$, which is also drawn in figure 8(*c*). Degenerate fixed points are points where $P(\sigma_0)$ just touches the line $\sigma_T = \sigma_0$ with a slope of 1, tangentially (i.e. nCE = 0 there). If there are no intersections of $P(\sigma_0)$ with the line $\sigma_T = \sigma_0$, then there are no integral curves of period T of (2.7*a*). There may, however, be integral curves of (2.7*a*) of period mT ($m > 1$) corresponding to fixed points of m applications of the Poincaré map.

The technique of analysis of time periodic examples is as follows. First, we integrate (2.7*a*) for the range of initial conditions. Next, we check the Poincaré map, which will look like figure 8(*c*) for intersections of $P(\sigma_0)$ with the line $\sigma_T = \sigma_0$. Assuming that there are such points, we know from the theory of circle maps that all initial conditions are eventually attracted to the stable fixed points. Then the out-of-plane and stretching dynamics of the microstructure is given simply by the nearby contraction exponent of these periodic points and the discrete time maps (3.11) and (3.12). We give examples that illustrate these ideas in §5.

4.2. *Robustness of the model in time-periodic flows*

The structural stability of the model system (2.7) for time-periodic flows differs from the case of simple flows that was analysed in §2.3. The reason is that the equations are non-autonomous rather than autonomous, and so the topology of the space where the vector field of (2.7) resides has changed. In the time-periodic case, we find that if (and only if) each fixed point of the Poincaré map is non-degenerate, then the qualitative nature of the dynamics is insensitive to small changes in the model equations that might account for Brownian motion, three-dimensionality, etc.

To see why this is so, consider a degenerate fixed point of the Poincaré map of (2.7*a*). The fixed point is degenerate because the Poincaré map intersects the line $\sigma_T = \sigma_0$ tangentially at the fixed point. A slight change in the model equations can shift the Poincaré map relative to the line $\sigma_T = \sigma_0$, yielding either no fixed point or two fixed points. This is analogous to the degenerate case in simple flows $D = 0$. Thus the presence of degenerate equilibria implies structural instability. To see why the existence of only non-degenerate equilibria implies structural stability, we refer the reader to Arnol'd (1983).

5. Examples

In order to demonstrate the application of our methods, we give three detailed examples of complex flow-microstructure systems. The types of flows we consider are open, steady and spatially inhomogeneous; closed, unsteady and homogeneous; and closed, steady and inhomogeneous. In doing these examples, we concentrate on the differences between the present analysis of the dynamics of microstructure and the analysis based on the assumption of simple flow. Techniques of the latter variety prove to be incapable of capturing the rich dynamics in these complex-flow examples.

5.1. *Microstructure in a boundary layer*

As a first example of the application of our methods, we consider the problem of the dynamics of microstructure in a particular boundary-layer flow. The outer flow of the problem is convergent, purely radial motion between two planar solid boundaries that intersect. Of course, this flow has a singularity at the point of intersection of the walls, but we are concerned instead with the motion in the boundary layer, away from the point of intersection. The solution of the steady fluid flow is due to Pohlhausen (1921); see also Rosenhead (1963, §V. 17). This example is particularly illustrative because we are able to do the analysis in closed form. At the end of the example, we will compare the simple and complex strong-flow criteria. For this particular example, the simple strong-flow criterion is not conservative enough. the interpretation of these criteria will be clear by the time we have finished with this example.

The outer flow for this problem is

$$U(x) = \frac{-U_0 l}{x}, \tag{5.1}$$

where $x > 0$ and U_0 is the speed when $x = 1$; the negative sign ensures convergent radial flow. The similarity variable is

$$\eta = \left(\frac{U_0 l}{\nu}\right)^{\frac{1}{2}} \frac{y}{x},$$

where ν is the kinematic viscosity. The boundary-layer solution, due to Pohlhausen, is

$$u = U(x)\, g(\eta), \quad v = \frac{-(U_0 l \nu)^{\frac{1}{2}}}{x} \eta g(\eta), \tag{5.2a,b}$$

where

$$g(\eta) = 3\tanh^2\left[\log(\sqrt{2}+\sqrt{3}) + \frac{\eta}{\sqrt{2}}\right] - 2$$

assumes values between 0 (at the solid wall) and 1 (at the outer flow).

The particle paths are straight lines $\eta = \eta_0$. This simplifies the calculation of the flow parameters; we obtain:

$$e(t) = \frac{\bar{e}}{x^2(t)}, \quad \bar{e} = U_0 l[g(\eta_0) + \eta_0 g'(\eta_0)], \tag{5.3a}$$

$$\gamma(t) = \frac{\bar{\gamma}}{x^2(t)}, \quad \bar{\gamma} = (U_0 l \nu)^{\frac{1}{2}} \eta_0 [2g(\eta_0) + \eta_0 g'(\eta_0)] - \frac{(U_0 l)^{\frac{3}{2}}}{\nu^{\frac{1}{2}}} g'(\eta_0), \tag{5.3b}$$

$$\omega(t) = \frac{\bar{\omega}}{x^2(t)}, \quad \bar{\omega} = (U_0 l \nu)^{\frac{1}{2}} \eta_0 [2g(\eta_0) + \eta_0 g'(\eta_0)] + \frac{(U_0 l)^{\frac{3}{2}}}{\nu^{\frac{1}{2}}} g'(\eta_0), \tag{5.3c}$$

where $x(t)$ is the x-coordinate of the particle path,

$$x(t) = (x_0^2 - 2lU_0\, g(\eta_0)\, t)^{\frac{1}{2}}. \tag{5.4}$$

Note that (5.4) does not make sense after the microstructure reaches the point of convergence of the solid boundaries, $x = 0$. The evolution equation (2.7a) is

$$\frac{\mathrm{d}\sigma}{\mathrm{d}t} = \frac{\bar{\omega}}{2x^2(t)} - \frac{G\bar{e}}{x^2(t)}\sin 2\sigma + \frac{G\bar{\gamma}}{2x^2(t)}\cos 2\sigma.$$

This equation can be made autonomous with respect to the new time τ, related to t through

$$\tau(t) = \int_0^t \frac{\mathrm{d}t}{x^2(t)}.$$

The new autonomous equation has a single, globally attracting orientation σ_+^* and a repelling orientation σ_-^* given by (2.12) with e, γ and ω replaced by the over-barred flow parameters. Qualitatively, the orientation dynamics are similar to what is shown in figure 4, but with a different time variable.

Next, we compare the two strong-flow criteria (2.16) and (3.13). To apply (3.13), we shall need the nearby contraction exponent at the globally attracting solution, which is easily computed as

$$\begin{aligned}\mathrm{nCE}\,[\sigma_+^*, T] &= (2G\bar{e}\cos(2\sigma_+^*) + G\bar{\gamma}\sin(2\sigma_+^*)) \int_0^T \frac{\mathrm{d}t}{x^2(t)} \\ &= \bar{D}^{\frac{1}{2}}\tau(T),\end{aligned}$$

where the over-barred discriminant is formed from the over-barred flow parameters, according to (2.12b). Thus the complex strong-flow criterion, equation (3.13), yields

$$\frac{\bar{D}^{\frac{1}{2}}\tau(T)}{T} > 2\alpha. \tag{5.5}$$

On the other hand, we evaluate the simple strong-flow criterion (2.16). We find that the discriminant D depends on time, through the relation

$$\frac{\bar{D}^{\frac{1}{2}}}{x^2(t)} = D^{\frac{1}{2}}.$$

Thus the simple strong-flow criterion at any instant of time is

$$\frac{\bar{D}^{\frac{1}{2}}}{x^2(t)} > 2\alpha. \tag{5.6}$$

Now let us perform the following thought experiment. Choose a time interval $[0, T]$, with $T/\xi < 1$, where $\xi = x_0^2/2lU_0\, g(\eta_0)$, so as to avoid the singularity in the flow field. Next fix the parameter α so that (5.5) with an equality sign is satisfied. Thus, over the time interval $[0, T]$, the maximum stretch of the microstructure is zero, as one can see from (3.12). Next we examine the simple strong-flow criterion. For the same value of α, it is a simple matter to show that the flow is weak (in the simple sense) for

$$t \in \left[0, \xi + \frac{T}{\log(1 - T/\xi)}\right],$$

and strong (in the simple sense) for

$$t \in \left[\xi + \frac{T}{\log(1 - T/\xi)}, T\right].$$

Thus, despite the fact that the microstructure appears to experience a strong flow in the simple sense for a finite sub-interval of $[0, T]$, there is no net stretch. Moreover, for a fixed value of ξ, the fraction of the interval $[0, T]$ in which the flow is strong (in the simple sense) varies from 0 to 100 % as the end point of the interval T varies from ξ to 0.

The interpretation of the two strong-flow criteria is now clear. The complex strong-flow criterion is a sufficient condition for the stretch of the microstructure over an interval of time. It is based on a true integral curve of the non-autonomous orientation equation. The simple strong-flow criterion is a sufficient condition for stretch of the microstructure at an instant of time. It is based on a particular assumed integral curve $\sigma(t) = \sigma_+^*$, a constant, which is an integral curve only for the autonomous equations, in general.

We remark that in this example (2.16) and (3.13) yield the same result if we use the time averaged value of $D(t)$ in (2.16). It should be emphasized that this is not generally the case. To analyse the microstructural behaviour correctly, one must apply (3.13).

Finally, it is clear that the complex strong-flow criterion for this example (5.5) shows a strong dependence on the particular time interval taken. In open-flow problems, the choice of this time interval is not so clear as in flows in which the flow parameters are periodic. In practice, this choice must be made so as to include in the time interval flow features that are important from the standpoint of orienting and stretching the microstructure. These features include close passage near to a stagnation point, or passage near streamlines connecting stagnation points or passage near solid boundaries, as in this example.

5.2. *Microstructure in time dependent stagnation point flow*

To demonstrate the relationship between the Poincaré map and the nearby contraction exponent in recirculating flows, we return to the third example of §3.1. We set $G = 1$, $\omega = 0$, $\gamma = 0$ and $e = -\cos(\epsilon t)$ in (2.7*a*). This example corresponds to a spatially homogeneous but temporally periodic flow with the stream function

$$\psi = -xy\cos(\epsilon t).$$

This flow is a simple stagnation point flow in which for half the period the y-axis is the outflow axis and the x-axis is the inflow axis. The flow reverses at every integer multiple of $\frac{1}{2}T$. The particle paths for this example are themselves periodic, being hyperbolae with asymptotes $x = 0$ and $y = 0$. Equation (2.7*a*) becomes

$$\dot{\sigma} = \sin(2\sigma)\cos(\epsilon t), \tag{5.7}$$

which has the solution

$$\sigma(t) = \tan^{-1}\left[\exp\left(\frac{2}{\epsilon}\sin(\epsilon t)\right)\tan(\sigma_0)\right]. \tag{5.8}$$

Note that the solution is periodic with period $T = 2\pi/\epsilon$ for any $\epsilon > 0$. If $\epsilon = 0$, however, the solution is not periodic:

$$\sigma_{\epsilon=0}(t) = \tan^{-1}[e^{2t}\tan(\sigma_0)].$$

In fact, every initial condition in the $\epsilon = 0$ (autonomous) system limits on the point $\sigma = \frac{1}{2}\pi$, whereas every initial condition in the $\epsilon > 0$ system is periodic. This is an important point. Despite the fact that the non-autonomous part of the orientation equation is $O(\epsilon^2)$ for ϵ small, the dynamics for $\epsilon > 0$ are in no way closely approximated by the 'nearby' autonomous system with $\epsilon = 0$ when $t = O(\epsilon^{-1})$.

Continuing with the example, we next compute the nearby contraction exponent,

$$\mathrm{nCE}\,[\sigma_0; T] = -\int_0^T 2\cos(\epsilon t)\cos(2\sigma(t;\sigma_0))\,\mathrm{d}t. \tag{5.9}$$

We substitute (5.8) into (5.9) and take the time interval T to be $2\pi/\epsilon$, the period of the flow parameters. We obtain $\mathrm{nCE}\,[\sigma_0; T] = 0$ for all σ_0. Thus the derivative of the Poincaré map is 1 everywhere. This matches the result of direct calculation of the Poincaré map from (5.8), which yields $P(\sigma_0) = \sigma_0$ for all σ_0.

Because the nearby contraction exponent is zero, we conclude from the complex strong-flow criterion (3.13) that there is no net stretch of the microstructure in this flow. This is an interesting point, because the presence of a stagnation point in a steady, homogeneous flow is normally indicative of a strong flow. It is the unsteady nature of this example that prevents this from being the case.

5.3. *Microstructure in the flow between eccentric rotating cylinders*

Finally, we consider the example of microstructure in the (Stokes) flow between eccentric rotating cylinders. The flow of a single-phase Newtonian fluid in this geometry has been studied extensively in the past, primarily owing to the important application to journal bearings. The first investigation by Reynolds (1986) neglected inertial effects and was restricted to the case of a narrow gap. Arbitrary gaps have since been considered by many authors; the most complete analysis is presented in Ballal & Rivlin (1977). Using a bipolar coordinate system, it is possible to solve the Stokes equations for the stream function. Our interest lies in the dynamics of microstructure suspended in this recirculating flow.

A single choice of operating parameters (cylinder diameters, eccentricity and rotation rates) suffices to demonstrate the application of the present analysis. Our primary goal is to explore the differences between our methods for the analysis of microstructural dynamics and the methods based on the assumption of simple flow. In this regard, it is easiest to compare directly the predictions of the two strong-flow criteria; (2.16) derived from the autonomous evolution equations that govern the dynamics of microstructure in simple flows, and (3.13), which we derived from the non-autonomous evolution equations that arise in complex flows. We observe the startling result that there are particle paths in the flow along which the simple strong-flow criterion predicts there is no particle stretching despite the fact that stretching does occur. We return to this point later.

To begin the analysis, suppose we have two cylinders arranged one within the other, but that the axes of the two cylinders although parallel do not coincide. The radius of the outer cylinder is R_1 and that of the inner cylinder is R_2. In rectangular coordinates, the axes of the inner and outer cylinders are located at $(l-\epsilon, 0)$ and $(l, 0)$, respectively, where ϵ is the eccentricity parameter. We define the bipolar coordinate system (ξ, η) through the relations

$$x = \frac{-b\sinh\xi}{\cosh\xi - \cos\eta}, \quad y = \frac{b\sin\eta}{\cosh\xi - \cos\eta}, \tag{5.10a, b}$$

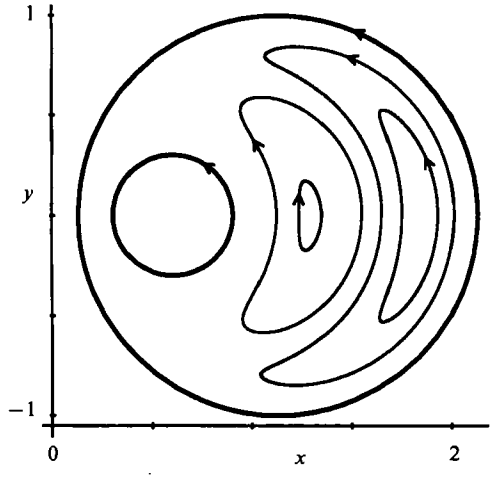

FIGURE 9. Representative particle paths computed for a particular case of the Stokes flow between eccentric rotating cylinders. The smaller cylinder, shown here in a cross-sectional view, rotates counterclockwise at 20 radians per unit time. The outer cylinder is co-rotating at 1 radian per unit time.

where b is a constant related to R_1, R_2 and ϵ. The stream function that solves the Stokes problem in this domain is given by

$$\psi = \frac{b[F_0(\xi)+F_1(\xi)\cos\eta]}{[(\cosh\xi\cos\eta-1)^2+(\sinh\xi\sin\eta)^2]^{\frac{1}{2}}}, \tag{5.11a}$$

where

$$F_0(\xi) = (A_0+C_0\xi)\cosh\xi+(B_0+D_0\xi)\sinh\xi, \tag{5.11b}$$

$$F_1(\xi) = A_1\cosh 2\xi+B_1\sinh 2\xi+C_1\xi+D_1. \tag{5.11c}$$

The geometrical relations of the constants b, A_i, B_i, C_i and D_i to the parameters R_1, R_2, and ϵ and the rotation rates of the cylinders Ω_1 and Ω_2 are given by Ballal & Rivlin.

Owing to the complicated nature of the stream function, we cannot integrate the equations

$$\dot{x}(t) = \frac{\partial\psi}{\partial y}(x,y), \quad \dot{y}(t) = -\frac{\partial\psi}{\partial x}(x,y) \tag{5.12}$$

analytically to obtain the particle paths; we must do so numerically. Consequently, it is not practical to compute the flow parameters analytically, and so we resort to finite-difference techniques. The particle paths are first obtained from (5.12) where the stream function is given by (5.11), and the numerical integration is performed using a standard fourth-order Runge–Kutta algorithm. Next, at each point along the (closed) particle path, we obtain the flow parameters e, γ and ω through finite (central) difference analogues of (2.5) and (2.6). Then we solve (2.7a) for the integral curves $\sigma(t;\sigma_0)$, which correspond uniquely to the particular initial orientations σ_0. The latter problem is solved using a standard predictor–corrector algorithm. The shape factor we use is $G = 0.98$. Next, we perform a simple integration to calculate the nearby contraction exponent for a given initial orientation, and finally analyse the dynamics.

We choose $R_1 = 1.0$, $R_2 = 0.3$ and $\epsilon = 0.525$ with rotation rates of $\Omega_1 = 1.0$

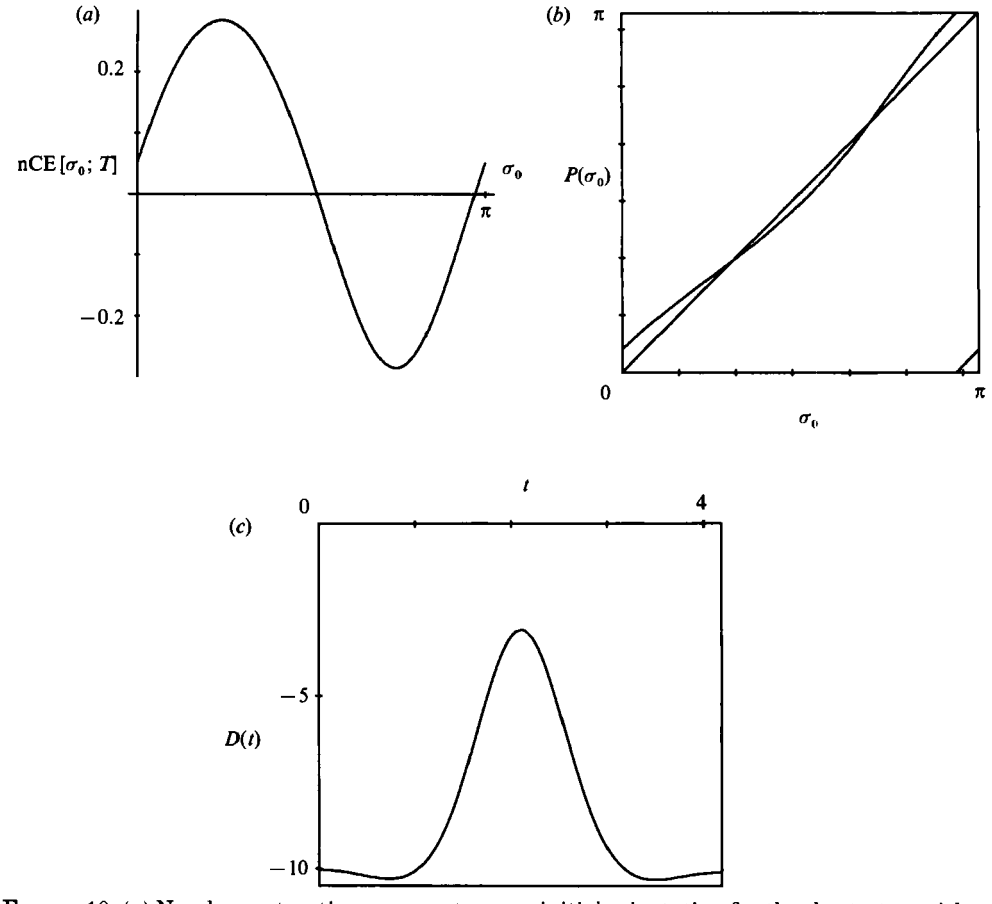

FIGURE 10. (*a*) Nearby contraction exponent versus initial orientation for the shortest particle path shown in figure 9, which begins at $x = 1.35$. (*b*) Poincaré map of the initial orientation for the shortest particle path shown in figure 9. (*c*) Time trace of the discriminant evaluated along the shortest particle path shown in figure 9.

$\Omega_2 = 20.0$, both counterclockwise. This choice of parameters corresponds to figure 14(*e*) of Ballal & Rivlin. In this interesting flow situation, there are two large eddies between the cylinders. In figure 9, we show some representative particle paths in the flow, all of which are closed curves in the (x, y)-plane.

We investigate the dynamics of microstructure that follow the shortest particle path of those shown in figure 9, which begins at $x = 1.35$. We follow the procedure outlined above, and obtain the nearby contraction exponent for the entire range of possible initial orientations, which is plotted in figure 10(*a*). One observes that nCE$[\sigma_0; T]$ is both positive and negative over the set of initial orientations σ_0, as we expect for reasons discussed in §4.1. The Poincaré map, $\sigma_T = P(\sigma_0)$ versus σ_0 also takes the expected form, as shown in figure 10(*b*). Note that there is a single unstable fixed point at approximately $\sigma_0 = 2.17$ radians and a single stable fixed point at approximately $\sigma_0 = 0.96$ radians. From the discussion of §4, we know that all initial orientations are attracted to the periodic integral curve that passes through $\sigma = 0.96$, i.e. the periodic integral curve is a stable (global) attractor. The nearby contraction exponent evaluated on the stable attractor is nCE$[0.96, T] = 0.27$, and the period of the flow parameters on this particle path is computed to be $T = 4.19$.

Thus, the complex strong-flow criterion, equation (3.13), allows us to conclude that there is stretch of the microstructure that follows the attracting periodic integral curve whenever $\alpha < \alpha_{\text{crit}} = 0.032$, that is to say whenever the spring constant α is weaker than α_{crit}.

Note that there are other (non-periodic) integral curves, in particular one for which $\sigma_0 = 0.77$ radians, that have a larger critical α. However, since all integral curves approach the globally attracting periodic integral curve, it seems more sensible to define α_{crit} as the critical spring constant on the attracting periodic integral curve. Thus we have shown that on this particle path there is an attracting periodic integral curve on which stretch of the microstructure takes place whenever $\alpha < 0.032$. As we now show, one could not come to this conclusion on the basis of the simple strong-flow criterion.

Recall that the simple strong-flow criterion is based on the discriminant D, which is formed from the flow parameters. Because this example flow is inhomogeneous, D changes along the particle path. Numerically, we have computed $D(t)$ and found it to be everywhere negative in the interval $[0, T]$ along this particle path; a plot of the time trace of D is given in figure 10(*c*). Thus, by the simple strong-flow criterion, equation (2.16), one would expect no stretch of the microstructure even if $\alpha = 0$! But this is not the case, as we have shown.

We can relate this result to the gallery of examples in §3.1. There we found that stability of unsteady disturbance evolution equations is not determined by the eigenvalues of the matrix associated with the linearized equations. The simple strong-flow criterion derived in §2.2 is based on the eigenvalue (in the ρ-direction) of the matrix associated with the linearization at an equilibrium orientation. Thus the simple strong-flow criterion cannot be expected to apply when the linearization of (2.7) is time dependent, i.e. in a flow that is unsteady in a Lagrangian sense, or as seen from the moving microstructure.

Within the context of this example, we have investigated the dynamics of microstructure that follow other particle paths. In every case we have examined, we find either a single periodic attracting integral curve, or no attractor of the same period as the particle path. For elements of the microstructure that pass close to the free stagnation points in the interior of the flow (there are two such points) we find there are periodic integral curves of the orientation that are ferociously attractive.

6. Conclusions

We have examined the dynamics of microstructure in complex two-dimensional fluid flows. We began by deriving the evolution equations for the conformation with respect to coordinates. Next we reviewed the range of possible behaviour in the case when the flow field is simple. When we moved on to consider the dynamical problem in complex flow fields, we found that the nature of the flow fields introduced much richer dynamics by changing the microdynamical evolution equations from autonomous to non-autonomous. This was clear in the examples of §§3.1 and 5. It was necessary to develop carefully the notion of attraction (or stability) of a conformation that was applicable to the problem. This led to a complex strong-flow criterion that is unrelated to conventional (simple) strong-flow criteria developed through the study of simple flows, as well as to an understanding of the dynamics as a whole. We were able to obtain additional results concerning orientation dynamics for the class of problems in which the influence of the flow on the microstructure is periodic in time.

In the past, researchers have approached complex-flow problems by looking at them as sequences of simple flows. We have attempted to demonstrate that the non-autonomous nature of the conformation evolution equations in complex flows leads to fundamentally different, history-dependent behaviour that cannot be approximated by autonomous behaviour, as some have attempted. Even in slowly-varying flow fields, the history dependent behaviour of the microstructure conformation is manifest.

A.J.S. would like to thank U. F. González for several interesting discussions on this work. This work was supported, in part, by a grant from the Office of Naval Research, and, in part, by the California Institute of Technology through the award of a Chaim Weizmann Research Fellowship in Applied Mechanics to A.J.S. S.W. would like to acknowledge a Young Investigator award from the Office of Naval Research and a Presidential Young Investigator award from the National Science Foundation.

Appendix. Relation of the present analysis to conventional dynamical stability analysis

In this Appendix, we discuss how our analysis of the microdynamical equations relates to some conventional techniques of analysis of dynamical systems. These remarks are intended for those readers with a deeper interest in dynamical systems. For background information on this broad subject, see Arnol'd (1973) or Guckenheimer & Holmes (1983). A particularly helpful discussion is available in Goldhirsch, Sulem & Orszag (1987).

We begin with a quick review of the standard analysis of the stability of a general integral curve in a one-dimensional ordinary differential equation. Given such an equation $\mathrm{d}x/\mathrm{d}t = f(x,t)$, and an integral curve $x = \xi(t)$, we investigate the dynamics relative to the integral curve by defining the variable $y(t)$ through $x = \xi(t) + \nu y(t)$, where ν is a parameter. The evolution equation for y is then

$$\frac{\mathrm{d}y}{\mathrm{d}t} = \frac{1}{\nu}[f(\xi(t)+\nu y(t),t) - f(\xi(t),t)]. \tag{A 1}$$

Taking the limit as ν approaches zero, we obtain the linearization

$$\frac{\mathrm{d}y}{\mathrm{d}t} = \frac{\partial f}{\partial x}(\xi(t),t)\, y(t). \tag{A 2}$$

The solution of this equation may be written as

$$y(t_2) = M[t_2,t_1]\, y(t_1), \tag{A 3}$$

where $t_2 > t_1$ and

$$M[t_2,t_1] = \exp \int_{t_1}^{t_2} \frac{\partial f}{\partial x}(\xi(t),t)\, \mathrm{d}t. \tag{A 4}$$

A suitable Lyapunov function for the integral curve $x = \xi(t)$ is simply $f(y) = y^2(t)$. We have stability whenever $f(y(t_2)) < f(y(t_1))$ for $t_2 > t_1$, that is to say whenever

$$y^2(t_2) = M^2[t_2,t_1]\, y^2(t_1) < y^2(t_1). \tag{A 5}$$

Thus the integral curve $x = \xi(t)$ is stable over the interval $[t_1,t_2]$ when $M^2[t_2,t_1] < 1$. The domain of attraction of the integral curve $x = \xi(t)$ over the interval $[t_1,t_2]$ is

found as follows. We keep the same Lyapunov function, but now we use the solution of the nonlinear equation (A 1) rather than the linearized form (A 3). The solution of (A 1) for ν not necessarily small may be written formally as

$$y(t_2) = N[t_2, t_1, y(t_1)]. \tag{A 6}$$

The basin of attraction of $x = \xi(t)$ is then defined to be the set of $y(t_1)$ such that

$$N^2[t_2, t_1, y(t_1)] < y^2(t_1) \tag{A 7}$$

analogous to (A 5). In specific examples, the basin of attraction may or may not be an easy set to find.

Our analysis of (2.7 *a*) is similar in some respect to the analysis just presented but different in others. In §3.2, we begin by solving the nonlinear disturbance evolution equation, which yields (3.6) analogous to (A 6), above. Rather than linearizing the disturbance evolution equation, we linearize its solution to obtain (3.9) analogous to (A 4). Thus for ν (of the prior analysis) small, $\epsilon(t)$ of §3.2 is analogous to $\nu y(t)$. For general $\nu, \delta(t)$ of (3.1) is the analogue of $\nu y(t)$.

The stability criterion (A 5) becomes

$$e^{-2nCE[\sigma_0;T]} < 1 \quad \text{or} \quad nCE[\sigma_0;T] > 0.$$

This is obtained by consideration of the Lyapunov function $f(\delta) = \delta^2(t)$. Because we began by solving the nonlinear disturbance evolution equation, it is a simple matter to find the basin of attraction of an attracting integral curve. We make use of (3.6) in (A 7) and the monotonicity of the tangent and arctangent functions. This yields

$$\{2\tan^{-1}[e^{-CE[\sigma_0,\sigma_0+\delta_0;T]}\tan(\tfrac{1}{2}\delta_0)]\}^2 < \delta_0^2,$$

whenever $CE[\sigma_0, \sigma_0+\delta_0; T] > 0$. This defines the basin of attraction of the integral curve $\sigma(t;\sigma_0)$ over the time interval $[0, T]$.

We remark that in the stability analysis, it is important to note that stability is related to the eigenvalues of the map M and not to the eigenvalues of the linearized equation, in general (see §3.1 for examples of what can happen if this is not taken into account). The reason for this is that we are considering the stability of a time dependent integral curve $x = \xi(t)$. In the special case when ξ and f do not depend on time, then $M[t_2, t_1] = \exp[\partial f/\partial x(\xi)(t_2 - t_1)]$, and stability is determined by the eigenvalues of the linearized equations, assuming their real parts are different from zero, of course.

An additional remark about Lyapunov exponents is in order. These numbers are particularly useful for characterization of attractors on which the motion is ergodic, i.e. when the motion eventually forgets its initial condition. For our generic one-dimensional system, the Lyapunov exponent is defined to be

$$\mu \equiv \lim_{t_2 \to \infty} \frac{1}{t_2 - t_1} \log \|M[t_2, t_1]\|. \tag{A 8}$$

The analogous definition for the orientation problem is

$$\mu \equiv \lim_{T \to \infty} \frac{1}{T} \log e^{-nCE[\sigma_0;T]} = \lim_{T \to \infty} \frac{-nCE[\sigma_0;T]}{T}.$$

If, for example, $\sigma(t;\sigma_0)$ is a periodic integral curve of period τ, then the corresponding Lyapunov exponent is $\mu = -nCE[\sigma_0;\tau]/\tau$. Thus, the periodic integral curve is stable for $nCE[\sigma_0;\tau] > 0$, as we already know.

In open-flow problems, or rather in problems where the flow parameters are not periodic in time, the Lyapunov exponent seems not to be a useful diagnostic quantity. The reason is that in two-(space) dimensional fluid flows, regions of relatively strong flow tend to be separated by large regions of relatively weak flow. Thus we expect nCE to be very different from zero only over finite time intervals. Because the definition of the Lyapunov exponent involves a limit as the time interval goes to infinity, the Lyapunov exponents computed for open flows would probably be nearly zero, despite the fact that interesting dynamics may occur over finite time intervals.

REFERENCES

AREF, H. 1984 Stirring by chaotic advection. *J. Fluid Mech.* **143**, 1–21.

ARNOL'D, V. I. 1973 *Ordinary Differential Equations.* MIT Press.

ARNOL'D, V. I. 1983 *Geometrical Methods in the Theory of Ordinary Differential Equations.* Springer.

ASTARITA, G. 1979 Objective and generally applicable criteria for flow classification. *J. Non-Newt. Fluid Mech.* **6**, 69–76.

BALLAL, B. Y. & RIVLIN, R. S. 1977 Flow of a Newtonian fluid between eccentric rotating cylinders: inertial effects. *Arch. Rat. Mech. Anal.* **62**, 237–294,

BIRD, R. B., HASSAGER, O., ARMSTRONG, R. C. & CURTISS, C. F. 1987 *Dynamics of Polymeric Liquids, vol. 2, Kinetic Theory.* J. Wiley.

BRETHERTON, F. P. 1962 The motion of rigid particles in a shear flow at low Reynolds number. *J. Fluid Mech.* **14**, 284–304.

CHAIKEN, J., CHEVRAY, R., TABOR, M. & TAN, Q. M. 1986 Experimental study of Lagrangian turbulence in a Stokes flow. *Proc. R. Soc. Lond.* A **408**, 165–174.

DRESSELHAUS, E. & TABOR, M. 1989 The persistence of strain in dynamical systems. *J. Phys.* A: *Math. Gen.* **22**, 971–984.

GOLDHIRSCH, I., SULEM, P.-L. & ORSZAG, S. A. 1987 Stability and Lyapunov stability of dynamical systems: a differential approach and a numerical method. *Physica* **27** D, 311–337.

GUCKENHEIMER, J. & HOLMES, P. 1983 *Nonlinear Oscillations, Dynamical Systems, and Bifurcations of Vector Fields.* Springer.

HALE, J. 1969 *Ordinary Differential Equations.* J. Wiley.

HINCH, E. J. 1977 Mechanical models of dilute polymer solutions in strong flows. *Phys. Fluids* **20**, 522–530.

HOLMES, P. 1984 Some remarks on chaotic particle paths in time periodic three dimensional swirling flows, *Contemp. Maths* **28**, 393–404.

JAMES, D. F. & SARINGER, J. H. 1982 Flow of dilute polymer solutions through converging channels. *J. Non-Newt. Fluid Mech.* **11**, 317–339.

JEFFREY, G. B. 1922 The motion of ellipsoidal particles immersed in a fluid. *Proc. R. Soc. Lond.* A **102**, 161–179.

KAPER, T. J. & WIGGINS, S. 1989 Transport, mixing and stretching in a chaotic Stokes flow: the two roll mill. Preprint, California Institute of Technology.

KUHN, W. & KUHN, H. 1945 Bedeutung beschränkt Drehbarkeit für die Viskosität und Strömungsdoppelbrechung von Fadenmolekellösungen I, *Helv. Chim. Acta* **28**, 97–127.

LEAL, L. G. & HINCH, E. J. 1971 The effect of weak Brownian rotations on particles in shear flow. *J. Fluid Mech.* **46**, 685–703.

MARKUS, L. & YAMABE, H. 1960 Global stability criteria for differential systems. *Osaka J. Maths* **12**, 305–317.

NOLLERT, M. U. & OLBRICHT, W. L. 1985 Macromolecular deformation in periodic extensional flows. *Rheol. Acta* **24**, 3–14.

OLBRICHT, W. L., RALLISON, J. M. & LEAL, L. G. 1982 Strong flow criterion based on microstructure deformation. *J. Non-Newt. Fluid Mech.* **10**, 291–318.

POHLHAUSEN, K. 1921 Zur näherungsweisen Integration der Differentialgleichung der laminaren Grenzschicht. *Z. Angew. Math. Mech.* **1**, 252–268.

REYNOLDS, O. 1886 On the theory of lubrication and its application to Mr. Beauchamp Tower's experiments. *Phil. Trans. R. Soc. Lond.* **177** (1), 157–234.

ROSENHEAD, L. (ED.) 1963 *Laminar Boundary Layers*. Oxford University Press.

TANNER, R. I. 1976 A test particle approach to flow classification for viscoelastic fluids. *AIChE J.* **22**, 910–918.

TANNER, R. I. & HUILGOL, R. R. 1975 On a classification scheme for flow fields. *Rheol. Acta* **14** (11), 959–962.

WIGGINS, S. 1988 *Global Bifurcations and Chaos – Analytical Methods*. Springer.